Triple-stage India-Asia collision involving arc-continent collision and subsequent two-stage continent-continent collision

Jie Yuan [a], Chenglong Deng [a,b,*], Zhenyu Yang [c], Wout Krijgsman [d], Thubtantsering [e], Huafeng Qin [a,b], Zhongshan Shen [a], Yifei Hou [a,b], Shuai Zhang [a,b], Zhiqiang Yu [a], Pan Zhao [a,b], Liang Zhao [a,b], Bo Wan [a,b], Huaiyu He [a,b], Zhengtang Guo [f]

[a] *State Key Laboratory of Lithospheric Evolution, Institute of Geology and Geophysics, Chinese Academy of Sciences, Beijing 100029, China*
[b] *College of Earth and Planetary Sciences, University of Chinese Academy of Sciences, Beijing 100049, China*
[c] *College of Resources, Environment and Tourism, Capital Normal University, Beijing 100048, China*
[d] *Department of Earth Sciences, Utrecht University, Utrecht HD 3584, the Netherlands*
[e] *College of Science, Tibet University, Lhasa 850000, China*
[f] *Key Laboratory of Cenozoic Geology and Environment, Institute of Geology and Geophysics, Chinese Academy of Sciences, Beijing 100029, China*

ARTICLE INFO

ABSTRACT

The enigmatic geodynamic processes involved in the India-Asia collision shape our understanding of uplift and deformation of the Tibetan Plateau and the subsequent changes in the land-sea distribution pattern, monsoon-arid environments and biotic evolution in Central-Eastern Asia. However, the current geodynamic models dealing with the India-Asia collision history exhibit significant discrepancies in how, when and where exactly the collision of India with Asia occurred. Recently, we proposed a new hypothesis that favored the opening and closure of a North India Sea during the late Cretaceous to Paleogene. Here we present new additional paleomagnetic data from the red siliceous shales and cherts of the Sangdanlin Formation, which were deposited on the most distal continental margin of the Tethyan Himalaya terrane, i.e. the southern margin of the Neo-Tethys Ocean, during the middle Paleocene. The combination of our new and previously reported paleomagnetic data shows that the Tethyan Himalaya was at a paleolatitude of $14.1° \pm 1.9°$N during the interval 62.5–59.2 Ma and refines the maximum size of the North India Sea to about 2200 ± 500 km. Combining our geodynamic model with recently published paleomagnetic data from the Kohistan-Ladakh arc, we conclude that the India-Asia collision was a triple-stage process, which involved an arc-continent collision followed by a two-stage continent-continent collision. The arc-continent collision occurred at ca. 64 Ma between the Tibetan Himalaya (Tethyan Himalaya plus Greater Himalaya) and the Trans-Tethyan subduction zone at a paleolatitude of ~8°N. The initial continent-continent collision took place at ca. 61 Ma between the Tibetan Himalaya (plus the accreted Trans-Tethyan subduction zone) and Lhasa terranes at a paleolatitude of ~14°N. The final continent-continent collision occurred during 53–47 Ma between India and the Tethyan Himalaya, diachronously suturing the North India Sea from west to east. The triple-stage collision scenario is in agreement with the history of India-Asia convergence rates, and is reflected by the presence of three slab remnants below Tibet and India as documented by seismic tomographic imaging. Our updated collision scenario reconciles multidisciplinary evidence for the India-Asia collision and provides better constraints on the resulting paleoclimatic and paleoenvironmental changes in Central-Eastern Asia.

1. Introduction

The India-Asia collision and ensued intra-continental convergence resulted in the rise and growth of the Himalayas and Tibetan Plateau, with an area larger than 2.5 million km^2 and an average elevation greater than 4000 m (Allègre et al., 1984; Fielding et al., 1994; Yin and Harrison, 2000). This orogeny is of great significance for our understanding of continental collision dynamics (Molnar and Tapponnier,

1975; Allègre et al., 1984; Tapponnier et al., 2001; Royden et al., 2008; Ding et al., 2017), Tethyan paleogeography (Allègre et al., 1984; Zhu et al., 2022), oceanic geochemistry (Richter et al., 1992; Misra and Froelich, 2012), global climate change (Raymo and Ruddiman, 1992), and paleoecology (Su et al., 2019; Ding et al., 2020; Zhao et al., 2020) during the Cenozoic. The collision has profoundly reshaped Asian land-sea distribution and topography patterns (Ramstein et al., 1997; Zhang et al., 2004; Wang et al., 2008; Spicer et al., 2021; Yuan et al., 2021; Wang et al., 2022), which were widely linked to major changes in global oceanic geochemistry (Misra and Froelich, 2012) and global climate (Raymo and Ruddiman, 1992; Zhang et al., 2001; Guo et al., 2002). Subsequently, the ongoing convergence between India and Asia was believed to drive the formation of monsoon-arid environments (Guo et al., 2002; Guo et al., 2008; Clift et al., 2008) and biodiversity patterns (Su et al., 2019; Ding et al., 2020) in Asia. This orogenesis is also important for the testing of hypotheses for tectonics-climate connection, e.g., the Himalayan uplift-erosion hypothesis (Raymo and Ruddiman, 1992) and the drift-weathering hypothesis (Kent and Muttoni, 2013).

However, the manner in which the India-Asia collision occurred has remained a long-standing controversy for nearly 100 years (Argand, 1924; Molnar and Tapponnier, 1975; Allègre et al., 1984; Hodges, 2000; Yin and Harrison, 2000; Ding et al., 2005; Aitchison et al., 2007; van Hinsbergen et al., 2012; Hu et al., 2015; Jagoutz et al., 2015; Zhu et al., 2015; Xiao et al., 2017; Kapp and DeCelles, 2019). Significant discrepancies exist, between the many geodynamic scenarios of India-Asia collision that can be subdivided in two main groups: the single-stage collision and the two-stage collision scenarios. The classical single-stage collision model represents the continental Greater India model, which was described as the Paleocene India-Asia collision at ca. 60 Ma resulting from Neo-Tethyan oceanic lithosphere subduction along the southern margin of Asian continent. This model, however, requires large-scale subduction of Indian continental crust (e.g., Ingalls et al., 2016) for which robust evidence is lacking.

This complexity resulted in the development of several two-stage collision models that include different components and infer competing age constraints: 1) The island arc-continent collision model (Aitchison et al., 2007) signals the importance of an intra-oceanic arc within the India-Asia collision zone and proposes the collision of the Trans-Tethyan subduction zone (TTSZ) and India at ca. 50 Ma followed by the collision of the amalgamated arc-continent with Asia at ca. 40 Ma (Jagoutz et al., 2015; Westerweel et al., 2019); 2) The Greater India Basin hypothesis (van Hinsbergen et al., 2012, 2019; van Hinsbergen and Schouten, 2021) invokes an ocean basin between India and the Tibetan Himalaya during ca. 120–25 Ma and indicates an initial collision of the Tibetan Himalaya with Asia at ca. 60–50 Ma and a second collision of India with Asia at ca. 30–25 Ma; 3) The India-arc collision with the Xigaze backarc basin (Kapp and DeCelles, 2019) proposes the opening and closure of the Xigaze backarc basin, in which the initial collision of India with the hypothetical Xigaze ophiolite-forearc-arc terrane occurred at ca. 60 Ma, and then the collision of India (plus the amalgamated Xigaze ophiolite-forearc-arc terrane) with Asia at ca. 45 Ma. However, none of the above-mentioned collision models can fully account for the variations in the India-Asia convergence rates and reconcile the multidisciplinary evidence from geology, geophysics, geochemistry and paleontology associated with the India-Asia collision (Parsons et al., 2020). This fact suggests that a more comprehensive collision model fully involving arc-continent collision and continent-continent collision is required.

Recently, we proposed another two-stage model: 4) The North India Sea hypothesis (Yuan et al., 2021) that invokes the opening and closure of an ocean basin (e.g., the North India Sea) during ca. 75–48 Ma and documents a two-stage continent-continent collision scenario, first at ca. 61 Ma between the Tibetan Himalaya and Asia, and subsequently at ca. 53–48 Ma between India and the Tibetan Himalaya. Our scenario did not include an arc-continent collision phase, because the inferred timing of India-TTSZ collision at 60 Ma (Westerweel et al., 2019) was in

disagreement with our reconstruction, which suggested that any island arc-continent collision should have occurred before ca. 61 Ma (Yuan et al., 2021). Recently, however, Martin et al. (2020) reported robust and reliable paleomagnetic data obtained from Khardung volcanic rocks on the Kohistan-Ladakh arc in Ladakh, India indicating that the intra-oceanic TTSZ was in fact active at a paleolatitude of $8.1 \pm 5.6°N$ between 66 and 62 Ma.

These two new scenarios were published contemporaneously and therefore not yet integrated. It seems evident, however, that the incorporation of India-TTSZ collision at >62 Ma in the North India Sea scenario will solve several geodynamic inconsistencies and result in a new triple-stage model for the India-Asia collision history. Here, we first present additional paleomagnetic data from the red siliceous shales and cherts of the mid-Paleocene Sangdanlin Formation in the distal northern part of the Tethyan Himalaya terrane, to better define the paleo-latitudinal position of the 61 Ma-collision between the Tibetan Himalaya and Lhasa terranes and refine the maximum size of the North India Sea. Next, we incorporate the arc-continent collision of Martin et al. (2020) into our previous continental collision scenario of Yuan et al. (2021), which leads to an updated and more comprehensive triple-stage collision scenario that integrates an arc-continent collision and a subsequent two-stage continent-continent collision. Finally, we discuss the triple-stage North India Sea collision scenario with literature results on India-Asia convergence rates, mantle tomography, continental deformation, magmatism and ultra-high pressure metamorphism, sediment provenance, basin evolution, and faunal migration to reconcile the multiple lines of evidence for our new geodynamic model of India-Asia collision.

2. Geologic setting and sampling

In the central and eastern Himalaya, the Yarlung Tsangpo suture (Fig. 1A) represents the early Cenozoic collision zone between the Tethyan Himalaya and Lhasa terranes, and by definition between the Indian and Asian continents as well. In the western Himalaya, India and Asia are separated by the intra-oceanic Kohistan-Ladakh arc (Tapponnier et al., 1981; Beck et al., 1996) (Fig. 1A). The Kohistan-Ladakh arc contacts the Asian Karakoram terrane in the north with the Shyok suture and the Indian continent in the south with the Indus suture (Tahirkheli, 1979) (Fig. 1A). To the south of the Indus and Yarlung Tsangpo sutures, the Himalayan orogen is divided into four broadly continuous tecto-nostratigraphic units, including, from north to south, the Tethyan Himalaya, the Greater Himalaya, the Lesser Himalaya and the Sub-Himalaya terranes, which are separated by, from north to south, the South Tibet Detachment System, the Main Central Thrust, the Main Boundary Thrust and the Main Frontal Thrust, respectively (Le Fort, 1975; Hodges, 2000) (Fig. 1A). In our study, we will follow van Hinsbergen et al. (2012) who defined the Tibetan Himalaya as the combination of the Tethyan Himalaya and the Greater Himalaya.

The Tethyan Himalaya (Fig. 1A) structurally overlies the Greater Himalaya (Gansser, 1964; Hodges, 2000) and comprises Cambrian-Eocene sedimentary rocks and Permian, Triassic, lower Cretaceous and Eocene-Miocene plutonic rocks and mafic lavas that form the distal continental margin of India (Garzanti et al., 1987; Hodges, 2000; Martin, 2017). Moreover, in some places near the peak of the Himalaya, lower Paleozoic rocks contain regional metamorphic assemblages consistent with middle to lower amphibolite-facies conditions (Coleman, 1996; Hodges et al., 1996). No clear exposure of the base of the Tethyan Himalaya has been found (Hodges, 2000).

The Greater Himalaya (Fig. 1A) is structurally emplaced over the Lesser Himalaya (Hodges, 2000; Martin, 2017) and consists of high-grade metasedimentary and metavolcanic rocks and associated leucogranites (e.g., Hodges, 2000). The metasedimentary and metavolcanic rocks metamorphosed under amphibolite-facies conditions, frequently up to partial melting conditions, and are intruded by Cenozoic leucogranites (Hodges, 2000; Xu et al., 2021).
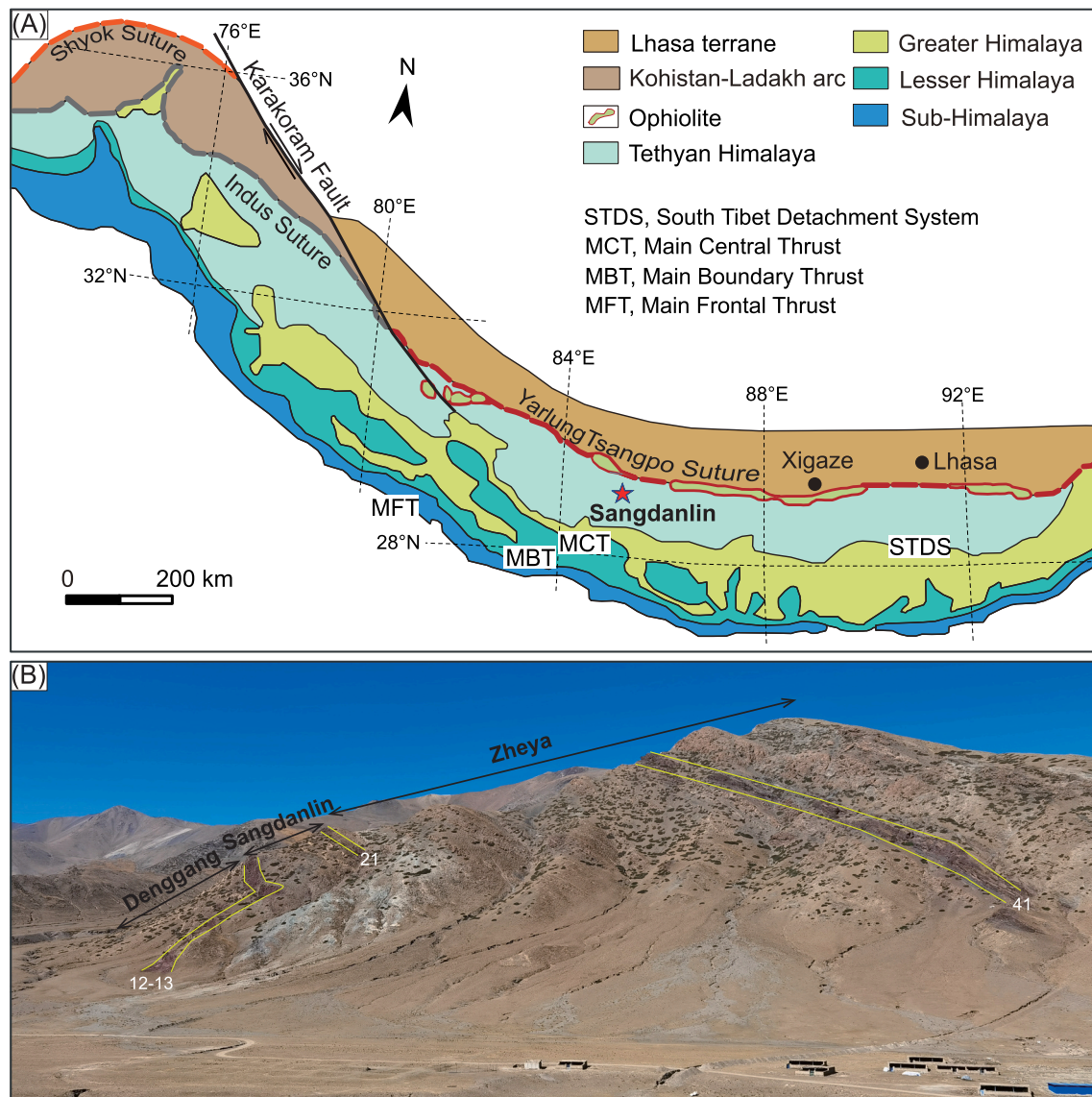
Fig. 1. (A) Geologic map of the Himalaya simplified from Yin (2006), showing the study region and location of the Sangdanlin section. (B) Panorama of the Sangdanlin section, looking to the west. The section comprises, from bottom to top, the upper Cretaceous–Paleocene Denggang Formation (Beds 1–10), the middle Paleocene Sangdanlin Formation (Beds 11–21) and the upper Paleocene Zheya Formation (Beds 22–49) (Hu et al., 2015, 2017).

The Lesser Himalaya (Fig. 1A) is structurally emplaced over the Sub-Himalaya (Hodges, 2000). The Lesser Himalaya comprises Paleoproterozoic to, in some places, Eocene-Oligocene sedimentary rocks (e. g., Hodges, 2000; DeCelles et al., 2004; Martin, 2017).

The Sub-Himalaya (Fig. 1A) is positioned between the Lesser Himalayan zone and the Main Frontal Thrust, which represents the most southern structure of the Himalayan orogen (DeCelles et al., 1998). The Sub-Himalaya comprises uppermost Paleocene or lower Eocene to lower Miocene sedimentary rocks of the Rawalpindi Group and weakly metamorphosed Miocene to Pleistocene synorogenic sedimentary rocks of the Siwaliks Group (e.g., DeCelles et al., 1998; Burbank et al., 1997; Hodges, 2000).

The Sangdanlin section (29°15.39′N, 85°15.02′E) in the Saga area, southern Tibet (Fig. 1B) represents the most distal continental margin of the northern Tethyan Himalaya and documents the first Asia-derived sediments deposited in the Tethyan Himalaya at ca. 60 Ma (DeCelles et al., 2014; Wu et al., 2014; Hu et al., 2015). This section is commonly divided into three formations (Ding et al., 2005; Hu et al., 2015, 2017) (Fig. 1B). The upper Cretaceous–Paleocene Denggang Formation (Beds 1–10) comprises yellow coarse quartzose sandstones intercalated with greyish-green silty sandstones and shales. Upward, the middle Paleocene Sangdanlin Formation (Beds 11–21) and the upper Paleocene Zheya Formation (Beds 22–49) consist of purplish-red siliceous shales, cherts, quartzose sandstone and volcaniclastic sandstones (Ding et al., 2005; DeCelles et al., 2014; Wu et al., 2014; Hu et al., 2015, 2017).

In this study, we conduct new detailed magnetostratigraphic and paleomagnetic investigations on the red siliceous shales and cherts of Beds 12–13 of the Sangdanlin Formation in the Sangdanlin section (Fig. 1B). In 2020, a total of 152 core samples were drilled from these fine-grained sedimentary rocks with sampling intervals of 0.05–0.3 m. All core samples were drilled with a portable drill and oriented with magnetic and sun compasses. Then, these samples were cut into standard specimens with a length of 2.2 cm for stepwise thermal demagnetization. The remaining samples were used for scanning electron microscopy observations and rock magnetic measurements. Finally, the results were combined with the previously published paleomagnetic data from 56 specimens of sub-units 12–13 of the Sangdanlin section and 30 specimens of the Mubala section (Yuan et al., 2021).

3. Paleomagnetism of the Sangdanlin red siliceous shales/cherts

3.1. Magnetic mineralogy

To identify the magnetic mineralogy of the Sangdanlin red siliceous shales/cherts, we investigated polished thin sections and measured hysteresis loops, isothermal remanent magnetization (IRM) acquisition curves and backfield demagnetization curves on the representative specimens using methods as described in Yuan et al. (2021). These scanning electron microscopy observations clearly indicate that the magnetic mineral assemblage of the Sangdanlin red siliceous shales/cherts consists of both detrital and chemical hematite grains (Fig. S1), which is consistent with our previous observations (Yuan et al., 2021). Additionally, all rock magnetic behaviors suggest the dominant contribution of high-coercivity hematite (Fig. S2), in agreement with our previous results from several sections in the area (Yuan et al., 2021). Component analyses of coercivity distributions (Kruiver et al., 2001) (Fig. S2) also show two components with different coercivities, indicative of two different assemblages of hematite grains interpreted as fine-grained chemical hematite and coarse-grained detrital hematite.

Stepwise thermal demagnetization of the three orthogonal IRM components (Lowrie, 1990) is a powerful method to identify the magnetic mineral assemblage of a specimen (e.g., Deng et al., 2013). To further determine the composition of magnetic mineralogy, six representative specimens were magnetized in successively smaller fields along three mutually orthogonal axes (Lowrie, 1990), which are 2.4 T along the Z-axis, 0.4 T along the Y-axis, 0.12 T along the X-axis, respectively, using a 2G Enterprises Pulse Magnetizer (2G660). These specimens were then subjected to progressive thermal demagnetization

up to ~685 °C at 10–100 °C intervals. Thermal demagnetization of the three-component IRM of these selected specimens show that the hard, intermediate and soft magnetization components unblock quickly about 685 °C (Fig. 2), also suggesting the dominance of high-coercivity hematite as the main magnetic remanence carrier.

3.2. Paleomagnetism

These scanning electron microscopy observations and rock magnetic results show that the Sangdanlin red siliceous shales/cherts contain both authigenic and detrital hematite grains with different morphological structures and coercivities (Figs. S1 and S2). Swanson-Hysell et al. (2019) suggest that the primary magnetization can be effectively isolated from co-occurring authigenic hematite by high-resolution thermal demagnetization because detrital hematite thermally unblocks in a narrow high-temperature range. Following this suggestion, our high-resolution thermal demagnetization up to 670–690 °C with 20–50 °C intervals from room temperature to 650 °C and with 3–5 °C intervals from 650 °C to 670–690 °C using a PGL-100 thermal demagnetizer of Qin et al. (2020) clearly reveals three magnetic components for most of the specimens of the Sangdanlin red siliceous shales/cherts (Fig. 3): low-temperature components (LTCs, 80–300 °C), middle-temperature components (MTCs, 300–650 °C) and high-temperature components (HTCs, 650–690 °C). The paleomagnetic data of this study were combined with those of Yuan et al. (2021) to obtain an overall mean direction for the red siliceous shales/cherts in the Sangdanlin section (Fig. 4).

The sample-mean direction of the LTCs is $D_g = 357.0°$, $I_g = +39.3°$, $k = 28.5$, $\alpha_{95} = 1.7°$, $n = 248$ (147 specimens from this study, and 101 specimens from Yuan et al. (2021)) before tilt correction, and $D_s = 3.9°$,
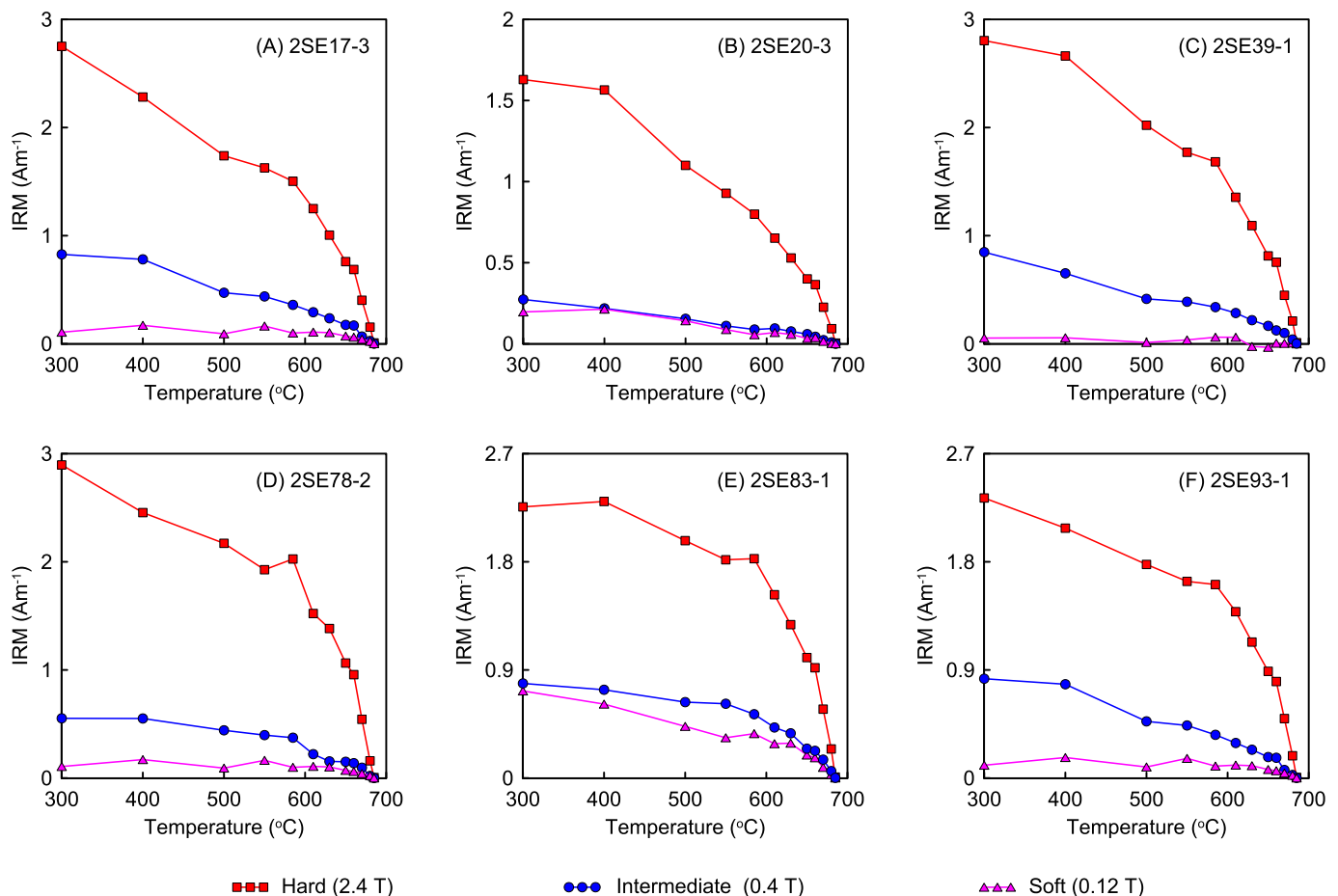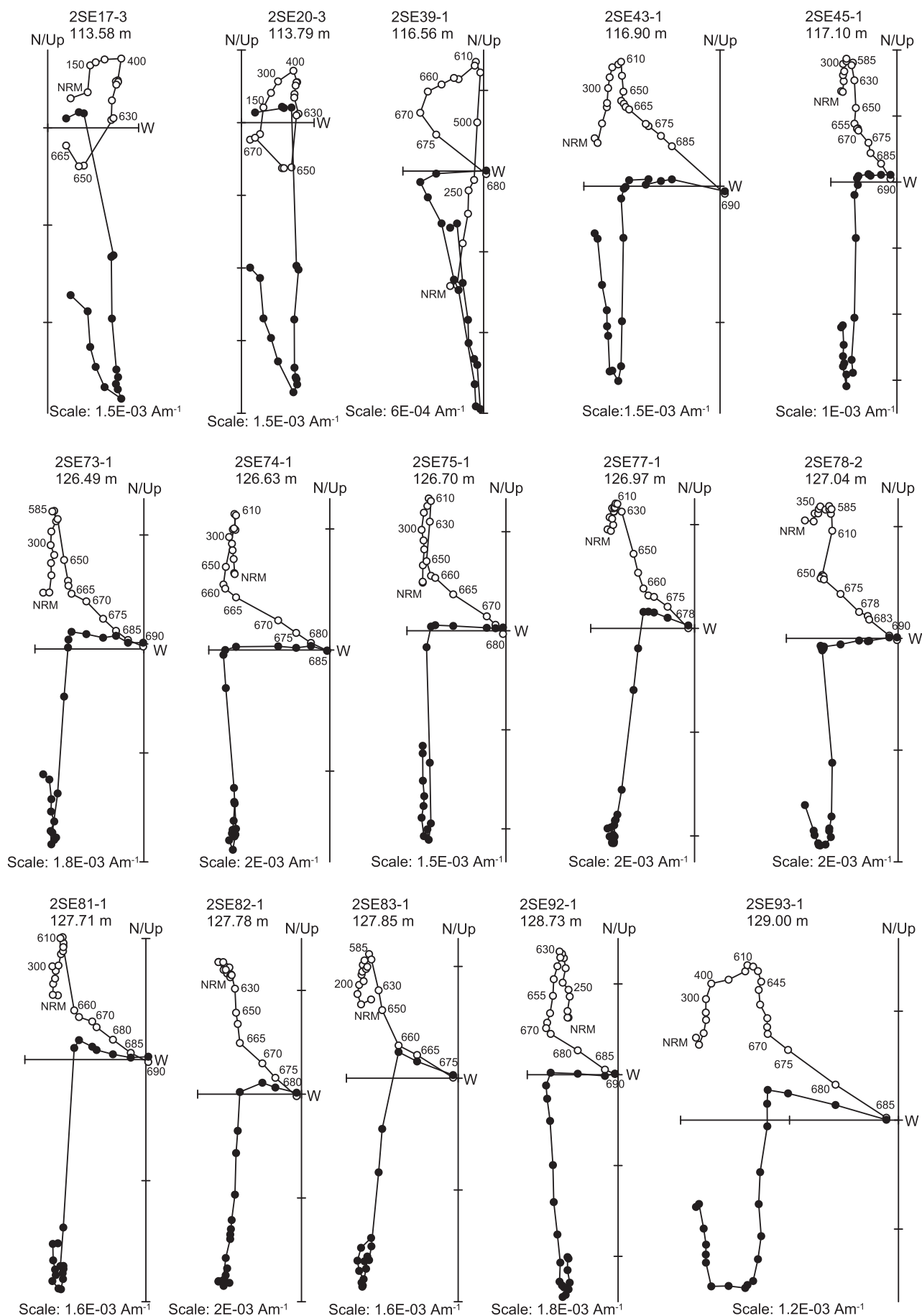

Fig. 2. Thermal demagnetization of the three-component IRM imparted with direct current fields of 2.4 T, 0.4 T, and 0.12 T along three perpendicular axes. The curves below 300 °C were cut for reasons of clarity.

(caption on next page)

$I_s = +5.8°$, $k = 29.8$, $\alpha_{95} = 1.7°$ after tilt correction (Fig. 4A, B). The sample-mean direction of the LTCs before tilt correction is close to the present geomagnetic field direction ($D = 0.5°$, $I = +46.2°$) of the sampling area, indicating that the LTCs are viscous remanent magnetizations. The sample-mean direction of the MTCs is $D_g = 180.1°$, $I_g = -16.9°$, $k = 90.6$, $\alpha_{95} = 1.0°$, $n = 238$ (142 specimens from this study, and 96 specimens from Yuan et al. (2021)) before tilt correction, and $D_s = 180.2°$, $I_s = +16.1°$, $k = 89.5$, $\alpha_{95} = 1.0°$ after tilt correction (Fig. 4C, D).

The HTCs could only be isolated in 76 specimens of our new sample set. In the other specimens, the HTCs could not be isolated, probably because the chemical remanent magnetization had overprinted the primary detrital remanent magnetization. The sample-mean direction of the HTCs is $D_g = 273.8°$, $I_g = -39.7°$, $k = 32.7$, $\alpha_{95} = 2.2°$, $n = 132$ (76 specimens from this study, and 56 specimens from Yuan et al. (2021)) before tilt correction, and $D_s = 255.1°$, $I_s = -19.6°$, $k = 37.8$, $\alpha_{95} = 2.0°$ after tilt correction (Fig. 4 and Table S1).

The MTCs (defined through 585–650 °C) revealed in our study could be carried by fine-grained chemical hematite grains, which are probably induced by orogenic hydrothermal fluids (Jiang et al., 2017, 2022; Swanson-Hysell et al., 2019) during a later episode of the Himalayan orogeny. The HTCs (defined through 650–690 °C) are considered the primary magnetizations in the studied Sangdanlin red siliceous shales/cherts, and this remanence is carried by coarse-grained detrital hematite grains.

3.3. Reliability of the paleomagnetic data

Our previous anisotropy of magnetic susceptibility results suggest that the Sangdanlin section experienced a 71° counterclockwise rotation relative to the Mubala section (Yuan et al., 2021). After correcting the HTCs from the Sangdanlin section for this local rotation, the sample-mean direction of the HTCs from the Sangdanlin section (76 specimens from this study, and 56 specimens from Yuan et al. (2021)) and the Mubala section (30 specimens from Yuan et al. (2021)) is $D_s = 180.5°$, $I_s = -19.4°$, $k = 33.1$, $\alpha_{95} = 2.0°$, $n = 162$ after tilt correction (Fig. 4G). A fold test is applied for the sample-mean HTCs of the Sangdanlin and Mubala sections. The significant increase of precision parameter k after tilt correction ($k_s/k_g = 8.07 > F (322,322) = 1.21$) indicates a positive fold test at the 95% confidence limit (McElhinny, 1964). In the fold test of McFadden (1990), the calculated values are $\xi_{(2)\text{in situ}} = 125.10$ in geographic coordinates and $\xi_{(2)\text{tilt corrected}} = 1.25$ after tilt correction, while the critical value is $\xi_C = 14.81$ at 95% confidence limit, also indicating a positive fold test. Applying the progressive unfolding of Watson and Enkin (1993) shows a maximum precision parameter ($k_{max} = 33.1$) at 100% unfolding, and a direction ($D_m = 0.5°$, $I_m = +19.4°$, $\alpha_{95} = 1.9°$) consistent with the mean direction after tilt correction (Fig. 4H). Moreover, the sample-mean direction of the HTCs of the Sangdanlin section passes the reversal test at 95% confidence level (B class, angle between all the normal and reversed directions $r_0 = 1.8° <$ critical Gamma $r_c = 5.3°$) (McFadden and McElhinny, 1990). The above-mentioned multiple lines of evidence demonstrate that the HTCs of the Sangdanlin section are primary.

3.4. Magnetostratigraphy

The HTCs determined from the Sangdanlin red siliceous shales/cherts of Beds 12–13 define two antipodal populations and represent both normal and reverse polarities, which (combined with the previous results by Yuan et al. (2021)) yield two magnetozones: the upper one

being reverse (R1); and the lower one, normal (N1) (Fig. 5). Correlation of the recognized magnetozones to the geomagnetic polarity timescale (Gradstein et al., 2020) was achieved by combining magnetostratigraphy, detrital zircon U-Pb geochronology, bentonite zircon U-Pb geochronology, and biostratigraphy. Firstly, biostratigraphic data suggest that Beds 9–13 of the Sangdanlin Formation correlate to Paleogene radiolarian zones RP4–RP6 (62.8–56.9 Ma) at low latitude (Hu et al., 2015), and that the overlying Zheya Formation corresponds to the upper part of the Paleocene calcareous nannofossil zone 7 (CNP7: 59.93–58.27 Ma) (Agnini et al., 2014; Hu et al., 2015). Secondly, a bentonite layer in Beds 47–48 of the Zheya Formation yields an LA-MC-ICPMS zircon U-Pb age of 58.5 ± 0.6 Ma (DeCelles et al., 2014). Thirdly, detrital zircon U-Pb geochronology data from Beds 14–16 show the youngest peak at ca. 60–58.5 Ma (Wu et al., 2014; DeCelles et al., 2014; Hu et al., 2015). Based on the independent biostratigraphic and geochronologic constraints and the nature of very low sedimentation rate of siliceous shales and cherts (e.g., several meters per million years; Matsuda and Isozaki, 1991), the magnetozones determined for the Sangdanlin red siliceous shales/cherts can be straightforwardly correlated to chrons C26r and C27n, which have been dated to extend from 62.2 to 59.2 Ma, and from 62.5 to 62.2 Ma, respectively, in the geomagnetic polarity timescale of Gradstein et al. (2020). Assuming relatively constant sedimentation rates in the red siliceous shales/cherts, Beds 12–13 of the Sangdanlin Formation in the Sangdanlin section are constrained to the time interval of 62.5–59.2 Ma (Fig. 5).

3.5. Inclination shallowing test and correction

The IRM anisotropy-based inclination shallowing correction, following the method of Hodych and Buchan (1994), yields a shallowing factor of ~0.7 for the red siliceous shales/cherts of the Sangdanlin Formation (Yuan et al., 2021). After using the IRM anisotropy-based inclination shallowing factor of ~0.7, the sample-mean inclination (Fig. 4G and Table S1) increased from 19.4° to 26.7°, resulting in an updated paleopole of 74.8°N/263.4°E, $A_{95} = 1.9°$, with a paleolatitude of $14.1° \pm 1.9°$N, which is well consistent with our previously obtained paleolatitude of $13.7° \pm 2.5°$N (Yuan et al., 2021); these are equivalent within errors.

4. Discussion

4.1. The size of Greater India

The size of Greater India (Argand, 1924) is a key issue that significantly influences tectonic models of the India-Asia collision, reconstructions of Mesozoic Gondwana and estimates of Himalayan crustal-shortening (Ali and Aitchison, 2005; van Hinsbergen et al., 2019). However, estimates for the extent of Greater India are highly variable, ranging from several hundred to about three thousand kilometers (Powell et al., 1988; Patzelt et al., 1996; Ali and Aitchison, 2005; Gibbons et al., 2012; Ingalls et al., 2016; Ding et al., 2017; van Hinsbergen et al., 2012, 2019; Meng et al., 2019; Yuan et al., 2021).

Powell et al. (1988) documented both the eastern Gondwana reconstruction and the India-Australia-Antarctica break-up history, which is widely considered to be definitive (Torsvik and Cocks, 2017). Furthermore, their assumed Greater India, with an extent of ~1700 km, extended to the Cape Range fracture zone, southwest of the Exmouth Plateau (Powell et al., 1988). Based on this reconstruction, Ali and Aitchison (2005), aware of continental origin of the Wallaby and Zenith Plateaus (Brown et al., 2003), suggested that eastern Greater India at
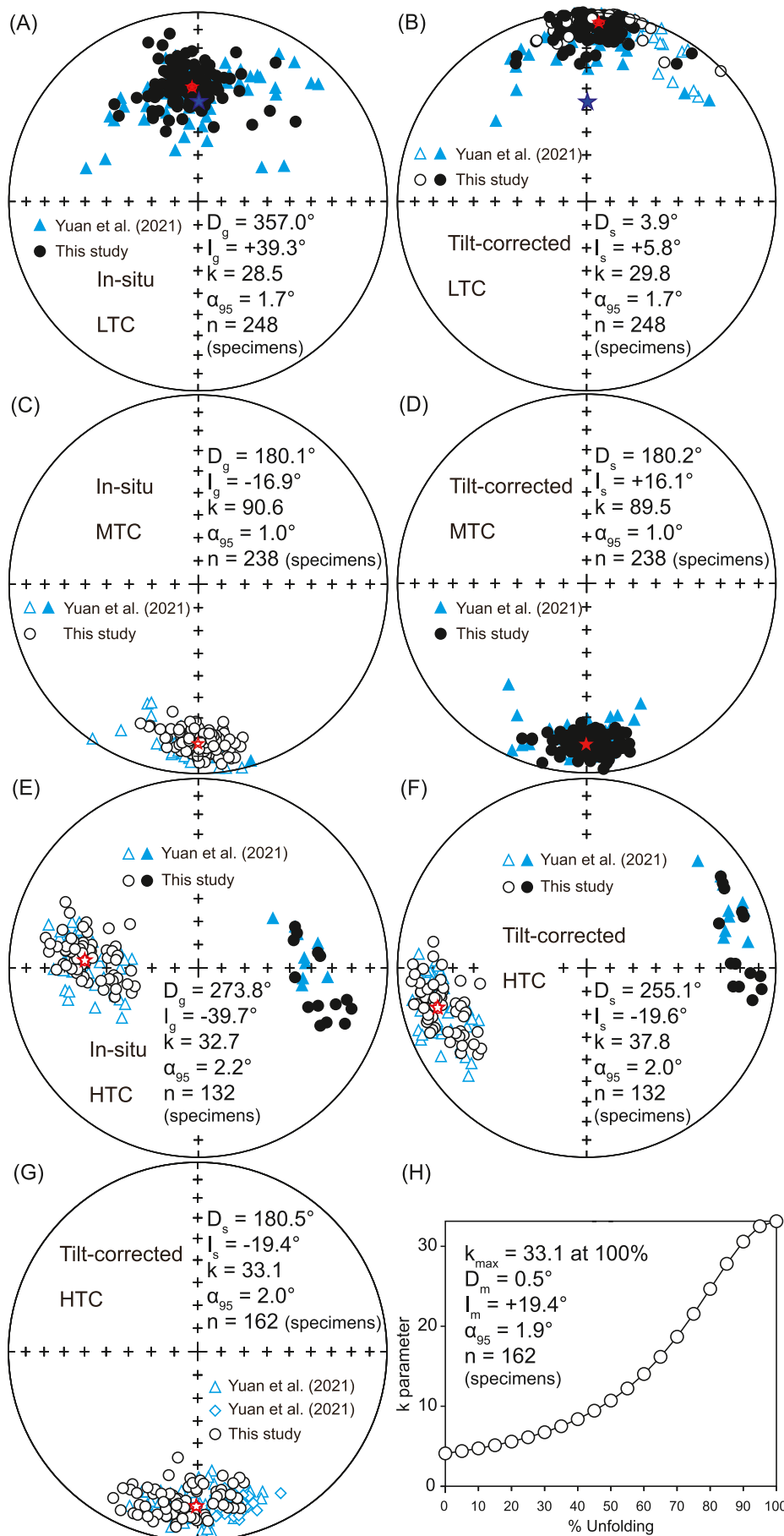
Fig. 4. Paleomagnetic results. (A–F) Equal-area projections of in situ (left) and tilt-corrected (right) paleomagnetic directions of all specimens of the Sangdanlin section. (A, B) LTCs (147 specimens (black circles) from this study, and 101 specimens (blue triangles) from Yuan et al. (2021)). (C, D) MTCs (142 specimens from this study, and 96 specimens from Yuan et al. (2021)). (E, F) HTCs (76 specimens from this study, and 56 specimens from Yuan et al. (2021)). (G) Equal-area projections of tilt-corrected HTCs of the Sangdanlin section (76 specimens from this study, and 56 specimens from Yuan et al. (2021)) after 71° counterclockwise rotation and of the Mubala section (30 specimens (blue diamonds) from Yuan et al. (2021)). (H) progressive unfolding of the mean HTC direction of the Sangdanlin section after 71° counterclockwise rotation and of the Mubala section. The blue stars in the (A) and (B) denote the present geomagnetic direction of sampling section. Red circles around the red stars in (A-G) denote the 95% confidence limit and mean directions. The mean directions were analyzed using classic Fisher statistics (Fisher, 1953). Solid and open symbols denote the lower and upper hemisphere projections, respectively. (For interpretation of the references to colour in this figure legend, the reader is referred to the web version of this article.)
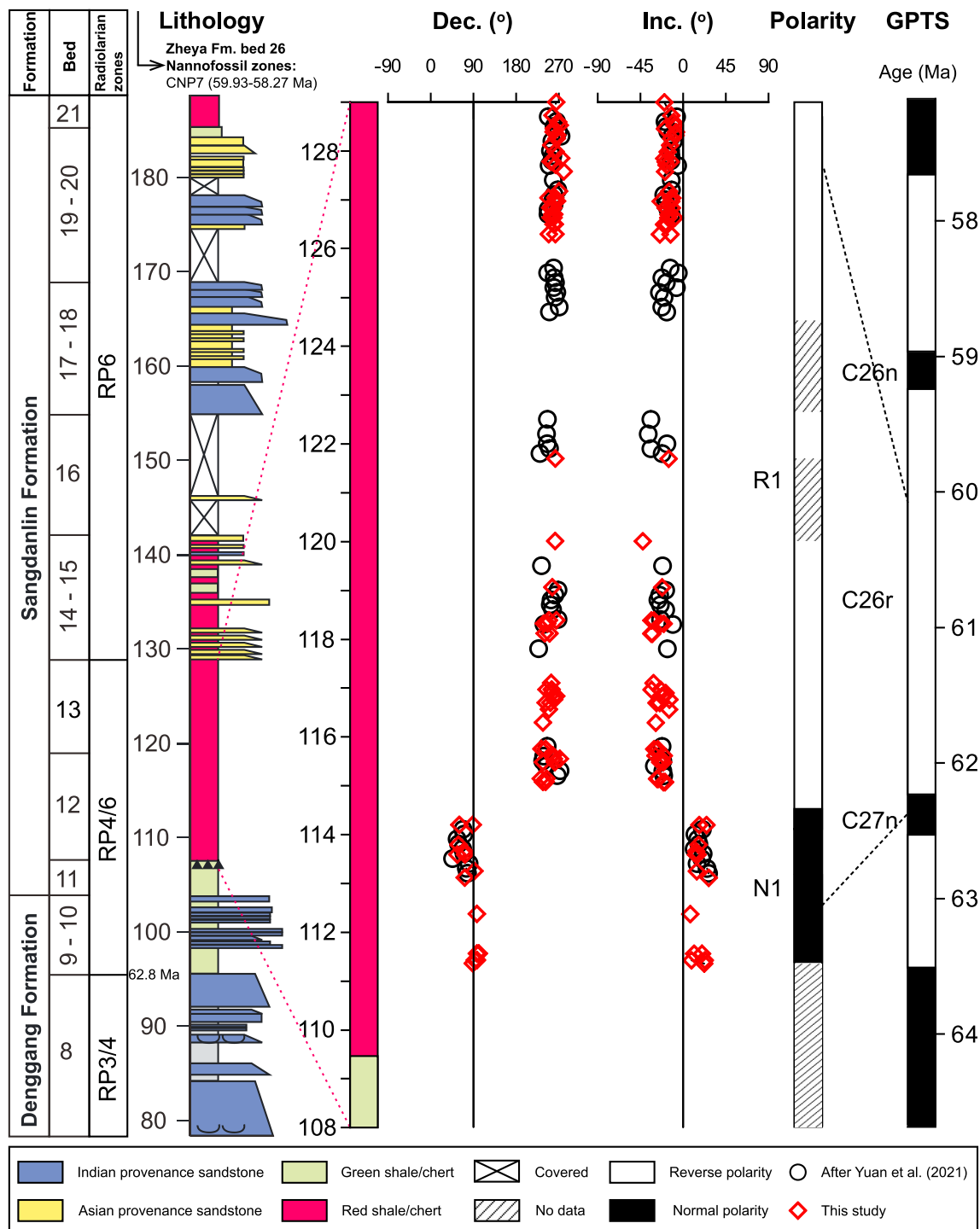
Fig. 5. Lithostratigraphy, biostratigraphy and magnetostratigraphy of the red siliceous shales/cherts (Beds 12–13) of the Sangdanlin Formation in the Sangdanlin section. The declination (Dec.) and inclination (Inc.) data of both this study (diamonds) and Yuan et al. (2021) (circles) are plotted as a function of stratigraphic level. Correlation of the recognized polarity sequence with the geomagnetic polarity timescale (GPTS) (Gradstein et al., 2020) is shown. Lithostratigraphy, lithology and biostratigraphy of the Sangdanlin section are after Hu et al. (2015, 2017). (For interpretation of the references to colour in this figure legend, the reader is referred to the web version of this article.)

most extended to the Wallaby-Zenith fracture zone. The presence of the Wallaby-Zenith fracture zone limits the north-south extent of eastern Greater India to <950 km, including the area of Himalayas (~250 km in north-south extent) north of the central Main Boundary Thrust. Subsequently, Gibbons et al. (2012) suggested that the major portion of Greater India had been located south of the Wallaby-Zenith fracture zone, thus excluding the previously proposed much larger Greater India.

Recent modeling results also do not support the existence of a continuous >3000 km continental Greater India (Liu et al., 2021).

Others suggested that Greater India only includes the subducted and tectonically shortened portions of the Indian continental crust during the India-Asia collision, thus excluding the area of Himalayas north of the central Main Boundary Thrust (Ding et al., 2017; Meng et al., 2019; Yuan et al., 2021). In this study, we follow the definition of Greater India

as proposed by Ding et al. (2017), who state that "*GI (Greater India) can thus be defined as the region to the north of the Indian plate, including under-thrusted Indian lithosphere and crustal shortening in the Himalayan mountain belt*". Yuan et al. (2021) provided an inclination-corrected Late Cretaceous paleopole and suggested that Greater India extended only 715 ± 374 km at ca. 75 Ma for the reference point (28.3°N, 85.3°E) (Fig. 6A). Moreover, only ~700 km crustal shortening was inferred from the geologic records in the Himalayan fold-thrust belts (DeCelles et al., 2002; Long et al., 2011). A seismic reflection profile across the western Himalaya implies that the Indian continent did not experience large-scale subduction (Gao et al., 2016). Consequently, it seems that a relatively small-sized Greater India (roughly less than 1000 km) should best be used for paleogeographic reconstructions (Klootwijk and Bingham, 1980; Ali and Aitchison, 2005; van Hinsbergen et al., 2012; Huang et al., 2015; Yang et al., 2015; Jagoutz et al., 2015; Ma et al., 2016; Bian et al., 2019; Qin et al., 2019; Martin et al., 2020; Yuan et al., 2021; Jadoon et al., 2022; Dannemann et al., 2022). In this study, we will use the 715-km-extent of Greater India paleomagnetically quantified by Yuan et al. (2021) to reconstruct the geodynamic process of the India-Asia collision.

4.2. The North India Sea hypothesis

Our recent paleomagnetic data sets from the Upper Cretaceous oceanic red beds (Chuangde Formation of the Cailangba section) and the Paleogene red siliceous shales/cherts (Sangdanlin Formation of the Sangdanlin and Mubala sections) in southern Tibet constrain the locations of the Tethyan Himalaya at paleolatitudes of $19.4° \pm 1.8°$S at ca. 75 Ma and $13.7° \pm 2.5°$N at ca. 61 Ma, respectively (Yuan et al., 2021). These data imply that the Tethyan Himalaya drifted northward with an anomalously high speed of ~260.1 mm/year, much faster than India with a speed of ~99.6 mm/year obtained by the apparent polar wander path (APWP) of India (Torsvik et al., 2012) during the same time period. The observations led Yuan et al. (2021) to hypothesize that the Tethyan-Greater Himalaya (i.e. the Tibetan Himalaya) rifted away from India and moved rapidly northward after ca. 75 Ma, thus generating the proposed North India Sea; and the Main Central Thrust was speculated to be the most logical position for the ancient rifting zone.

The combination of our new and previously published paleomagnetic data constrain the northern margin of the Tethyan Himalaya to an updated paleolatitude of $14.1° \pm 1.9°$N at ca. 61 Ma (Fig. 6C). In addition, this updated paleolatitude gives a slightly revised size of the North India Sea, which had a latitudinal width of 2178 ± 484 km (19.8° $\pm 4.4°$) at its central part and of 1342 ± 484 km (12.2° $\pm 4.4°$) at its western part at ca. 61 Ma (Fig. 6C).

There are several processes likely responsible for generating an oceanic basin at the northern continental margin of India during the 75–61 Ma time interval (Fig. 6A–C, Fig. 7 and Fig. 8). Firstly, the negative buoyancy of the long-time subducting Neo-Tethyan oceanic slab (Wan et al., 2019) resulted in dragging the Indian continent. Secondly, the existence of two parallel subduction zones between India and Asia probably since ca. 120 Ma could have generated a double slab-pull (Jagoutz et al., 2015). The combined pull of two subducting slabs continuously dragged the Indian continent. During ca. 90–80 Ma, the termination of intra-oceanic subduction at its eastern and western parts (Hall, 2012; Şengör and Stock, 2014) resulted in the reduction of the parallel trench of the TTSZ from ~10,000 km to ~3000 km in length, thus significantly accelerating the drift speed of the Indian continent after ca. 80 Ma (Jagoutz et al., 2015) (also see Fig. 8). Subsequently, the subducting Neo-Tethyan oceanic slab and intra-oceanic oceanic slab became older and more negatively buoyant (Jagoutz et al., 2015), which resulted in dragging of the Tibetan Himalaya from India, and thus leading to rifting of the Tibetan Himalaya away from India after ca. 75 Ma and generating the North India Sea (Fig. 6A–C, Fig. 7B and Fig. 8). The rifting may have been further induced by melting of the Indian passive continental margin lithosphere with upwelling of the Reunion plume (Kumar et al., 2007; Cande and Stegman, 2011; Paul and Ghosh, 2022).

In addition, during the expansion of the North India Sea, a contemporaneous foreland basin developed on the Lesser Himalaya of the northern passive margin of India (Critelli and Garzanti, 1994; DeCelles et al., 2004; Najman et al., 2005; Ravikant et al., 2011; Ding et al., 2016; Colleps et al., 2020), which could provide geologic evidence for the existence of the North India Sea.

4.3. The triple-stage India-Asia collision

Associated with the North India Sea hypothesis, Yuan et al. (2021) proposed a two-stage continental collision, first at ca. 61 Ma between the Tibetan Himalaya and Lhasa terranes, and subsequently at ca. 53–48 Ma between India and the Tibetan Himalaya, diachronously suturing the North India Sea from west to east.

Based on our previous two-stage continental collision scenario, the newly updated paleolatitude of the Tethyan Himalaya (that is, $14.1° \pm 1.9°$N at ca. 61 Ma reported in this study), and the early Paleocene paleolatitude of the intra-oceanic TTSZ constrained by paleomagnetic data from the Kohistan-Ladakh arc (that is, $8.1° \pm 5.6°$N at 66–62 Ma) (Martin et al., 2020), we propose a triple-stage India-Asia collision scenario, as illustrated in Figs. 6–8. This scenario involves 1) the arc-continent collision of the Tibetan Himalaya with the TTSZ at ca. 64 Ma, 2) the continent-continent collision between the Tibetan Himalaya (plus the accreted TTSZ) and Asia at ca. 61 Ma, and 3) the continent-continent collision between India and the Tibetan Himalaya at ca. 53–47 Ma.

4.3.1. The arc-continent collision of the Tibetan Himalaya with the TTSZ

The paleolatitudinal difference for the Tibetan Himalaya between ca. 75 Ma at 19.4°S (Yuan et al., 2021) and ca. 61 Ma at 14.1°N (this study) documents a high speed of ~263 mm/year for this terrane during the time interval between ca. 75 and ca. 61 Ma. In terms of this northward drift rate, it took ~11 million years to overlap with the paleolatitude of the TTSZ (8.1°N) (Martin et al., 2020), suggesting that the collision of the Tibetan Himalaya with the TTSZ occurred at the paleolatitude of ~8°N at ca. 64 Ma during the expansion of the North India Sea (Fig. 6B). The collision of the Tibetan Himalaya and the TTSZ provides a new alternative explanation for the arc-continent collision, slightly different from the traditional arc-continent collision that involved a near-equatorial collision of India and the TTSZ at ca. 60–50 Ma (Aitchison et al., 2007; Jagoutz et al., 2015; Westerweel et al., 2019; Martin et al., 2020). Moreover, we suggest that the Xigaze backarc basin, as proposed by Kapp and DeCelles (2019), could have been much smaller; and that the Xigaze arc of Kapp and DeCelles (2019) moved southward after 90–85 Ma, becoming a part of the TTSZ as suggested by Martin et al. (2020).

During the Early Cretaceous, the TTSZ extended nearly in an east-west direction and was dominantly located at low latitude (Zaman and Torii, 1999; Jagoutz et al., 2015; Westerweel et al., 2019; Martin et al., 2020; Zhang et al., 2020) (Fig. 6A). In the western Himalaya, the TTSZ was represented by the Kohistan-Ladakh arc (Martin et al., 2020); and in the east, by the Burma terrane (Westerweel et al., 2019; Zhang et al., 2022). In the central Himalaya, the presence of an intra-oceanic arc was originally proposed by Allègre et al. (1984) and was adopted by Aitchison et al. (2000). However, unambiguous geologic evidence for the existence of this arc remains unidentified due to its fragmentary nature in the accretionary mélange (Martin et al., 2020). More detailed and thorough geologic studies are necessary to reveal the evidence of the TTSZ in the central Himalaya.

4.3.2. The continent-continent collision between the Tibetan Himalaya (plus the accreted TTSZ) and Asia

After the arc-continent collision of the Tibetan Himalaya with the TTSZ, the Tibetan Himalaya (plus the accreted TTSZ) continued to travel northward to reach the southern margin of the Asian continent (the
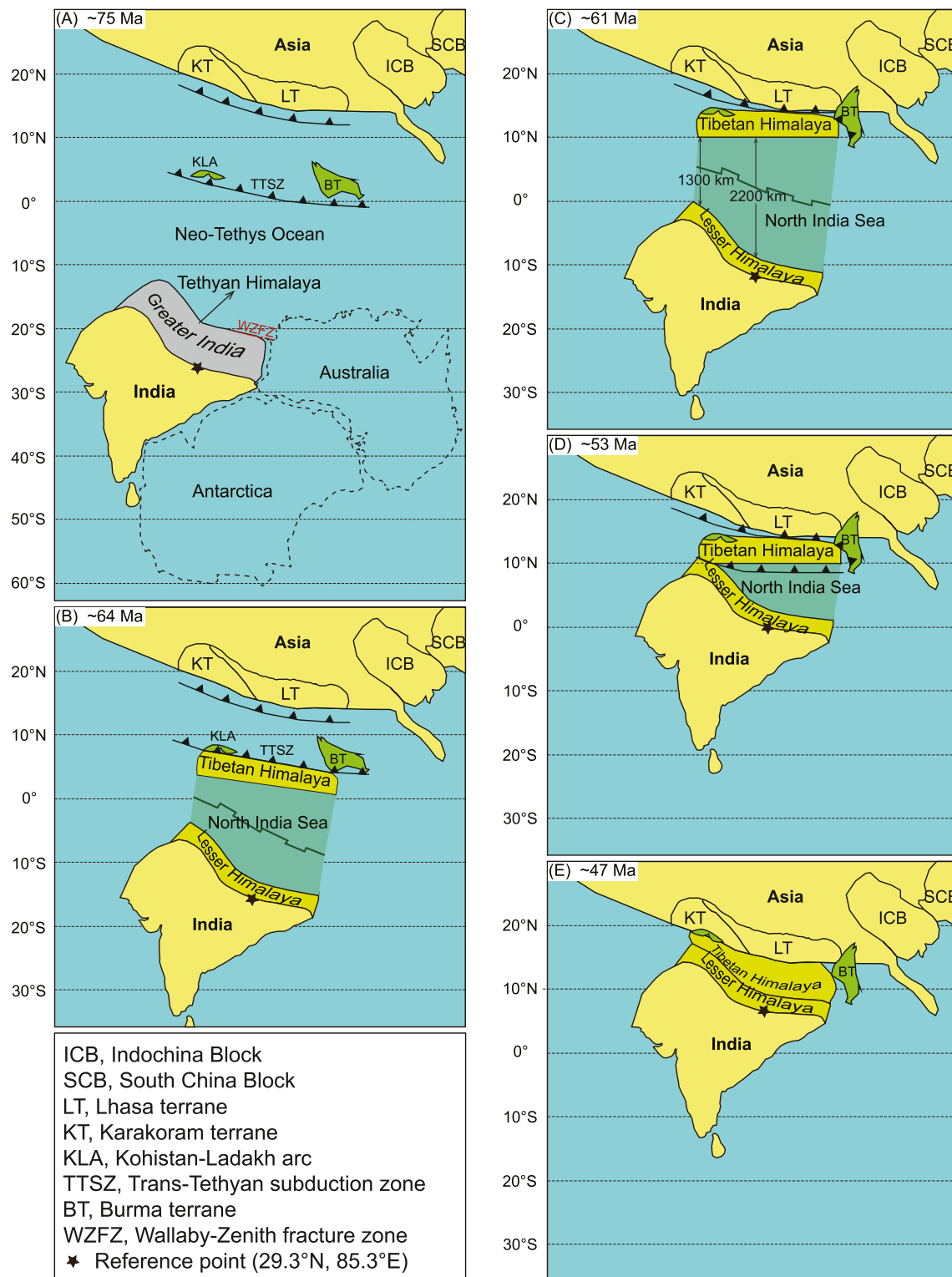
Fig. 6. The history of the India-Asia collision reconstructed on the basis of new paleomagnetic data of the Paleogene red siliceous shales/cherts (Sangdanlin Formation of the Sangdanlin section) in southern Tibet (this study), as well as published paleomagnetic data of the upper Cretaceous oceanic red beds (Chuangde Formation of the Cailangba section) and the Paleogene red siliceous shales/cherts (Sangdanlin Formation of the Sangdanlin and Mubala sections) in southern Tibet (Yuan et al., 2021), combined with results of the upper Cretaceous Khardung volcanics on the Kohistan-Ladakh arc in Ladakh (Martin et al., 2020), of the Cretaceous red beds on the Kohistan-Ladakh arc in Kohistan (Zaman and Torii, 1999), and of upper Cretaceous strata in the Wuntho Range, Burma (Westerweel et al., 2019). The paleogeographic reconstructions at ca. 75 Ma (A), ca. 64 Ma (B), ca. 61 Ma (C), ca. 53 Ma (D) and ca. 47 Ma (E) are shown. The Australian and Antarctic continents in (A) were reconstructed in the Gondwana framework only for determining the size of eastern Greater India. Position of the TTSZ was paleomagnetically constrained to a paleolatitude of 8.1° ± 5.6°N between 66 and 62 Ma (Martin et al., 2020), as shown in (B). *Trans*-Tethyan subduction zone (TTSZ) is the southern intra-oceanic subduction system proposed by Jagoutz et al. (2015). The Tibetan Himalaya proposed by van Hinsbergen et al. (2012) consists of the Tethyan Himalaya and the Greater Himalaya. (For interpretation of the references to colour in this figure legend, the reader is referred to the web version of this article.)
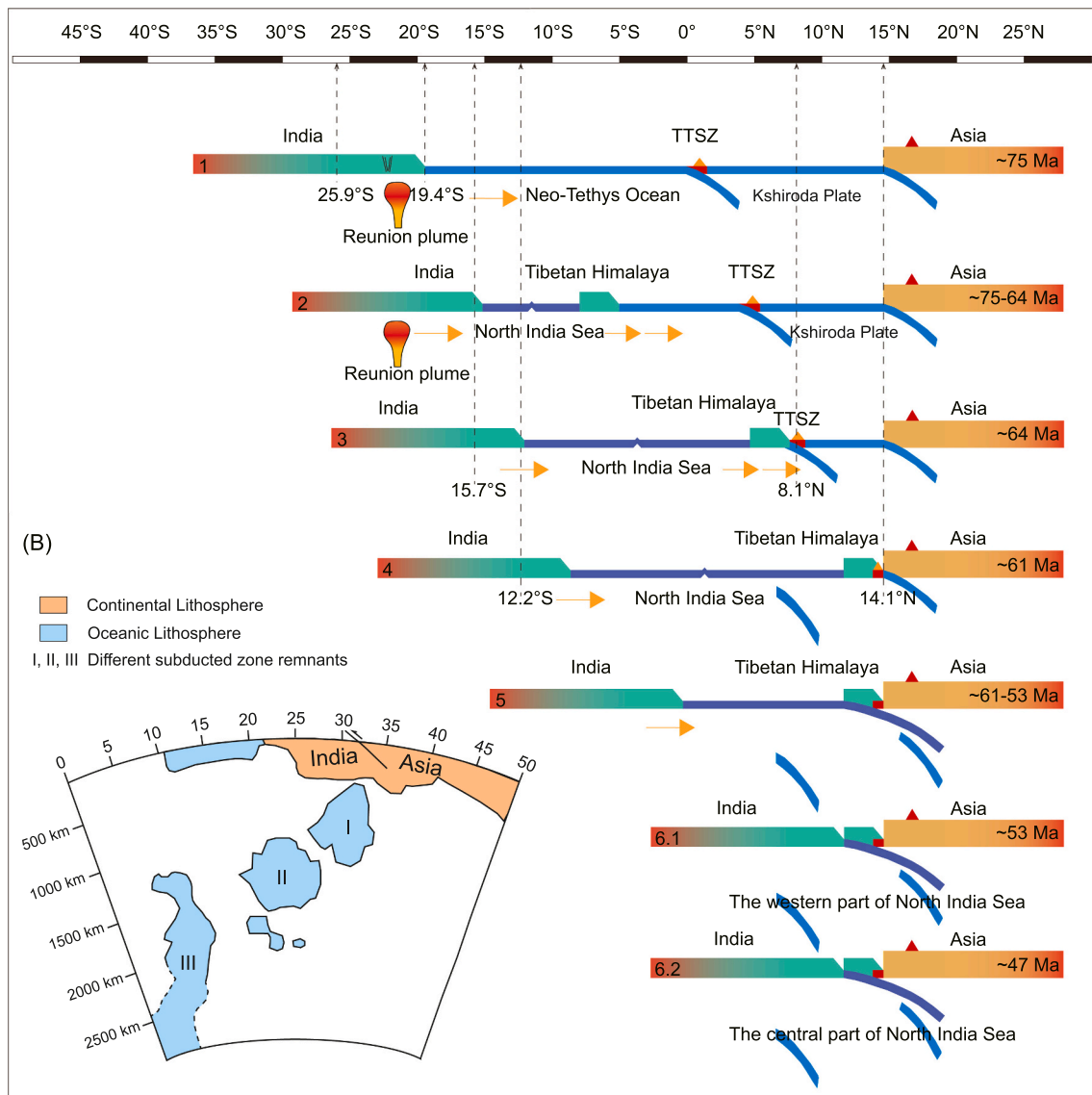
Fig. 7. (A) The India-Asia convergence history constrained by paleomagnetic data from this study, Yuan et al. (2021) and Martin et al. (2020). (B) Simplified version of tomographic image based on a synthesis of Fig. 4a-c of Van der Voo et al. (1999). In this study, the three high-velocity zones labelled I, II and III in (B) are considered the slab remnants of the North-India-Sea oceanic lithosphere, Neo-Tethyan oceanic lithosphere and intra-oceanic subducted oceanic lithosphere, respectively. Positions of the Trans-Tethyan subduction zone (TTSZ) are after Jagoutz et al. (2015) and Martin et al. (2020). The Kshiroda Plate proposed by Jagoutz et al. (2015) is the oceanic plate between the northern and southern subduction systems. The Tibetan Himalaya proposed by van Hinsbergen et al. (2012) consists of the Tethyan Himalaya and the Greater Himalaya.

Lhasa terrane). Yuan et al. (2021) previously re-evaluated all the paleomagnetic data of the Lhasa terrane based on the criteria proposed by Van der Voo (1990) and concluded that the southern margin of the Asian continent remained relatively stable at paleolatitudes of ~13.7°–15.7°N during the Cretaceous to Paleogene (Figs. 6–7). Our paleomagnetic results constrain the paleolatitude of the Tibetan Hima-laya at ~14.1°N during the mid-Paleocene, indicating an overlap with the Lhasa terrane within errors. This implies that the continent-continent collision between the Tibetan Himalaya (plus the accreted TTSZ) and Asia must have occurred at the paleolatitude of ~14°N at ca. 61 Ma (Figs. 6–7). Additionally, we agree with the suggestion of Martin et al. (2020) that this collision occurred along the Shyok-Yarlung Tsangpo suture zone, and not along the Indus-Yarlung Tsangpo suture zone (Fig. 1).

4.3.3. The continent-continent collision between India and the Tibetan Himalaya

At ca. 61 Ma the paleolatitude of the Tibetan Himalaya terrane overlapped that of the Lhasa terrane, thus the latitudinal width of the North India Sea can be determined to be about 1300 ± 500 km at its western part and about 2200 ± 500 km at its central part, respectively (Fig. 6C). Then, India continued to travel northward to close the North India Sea. Based on India's northward drift rates calculated by its APWP (Torsvik et al., 2012), it took ~8 million years to close its western part and ~ 14 million years to close its central part, respectively (Figs. 6–7). This diachronous episode of continent-continent collision between India and the Tibetan Himalaya thus occurred between ca. 53 and 47 Ma (Figs. 6–8). The Main Central Thrust could be the most logical preserved position for the required ancient subduction zone.
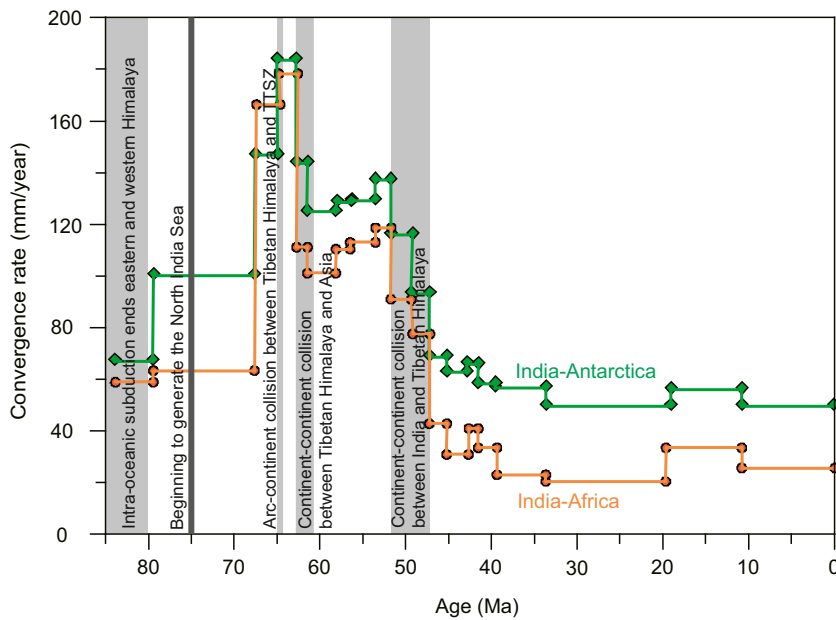
Fig. 8. The India-Asia convergence history documented by the spreading rates between India-Africa and India-Antarctica ridges (Cande and Stegman, 2011). Gray shading from left to right indicate key tectonic events: i) the India-Asia convergence rates began to increase at ca. 80 Ma after intra-oceanic subduction ended at its eastern and western parts during ca. 90–80 Ma (Jagoutz et al., 2015); ii) the Tibetan Himalaya terrane rifted away from India after ca. 75 Ma, generating the North India Sea (Yuan et al., 2021); iii) the arc-continent collision between the Tibetan Himalaya terrane and the intra-oceanic TTSZ occurred at ca. 64 Ma; iv) the continent-continent collision between the Tibetan Himalaya terrane (plus the accreted TTSZ) and Asia occurred at ca. 61 Ma; v) the continent-continent collision between India and the Tibetan Himalaya terrane occurred at ca. 53–47 Ma. TTSZ, Trans-Tethyan subduction zone.

4.4. Evidence for the triple-stage India-Asia collision process

4.4.1. Variations of the convergence rates between India and Asia

The triple-stage India-Asia collision scenario proposed in this study (Figs. 6–7) consistently explains the history of the India-Asia convergence rates (Cande and Stegman, 2011), which is characterized by two distinct pulses of rapid motion, separated by a notable slowdown (Pusok and Stegman, 2020) (also see Fig. 8). The combined slab-pull by two subducting slabs in the Neo-Tethyan double subduction systems and a reduction in length of the TTSZ from about 10,000 to 3000 km between 90 and 80 Ma (Jagoutz et al., 2015) were responsible for the rapid acceleration of India's motion after ca. 80 Ma.

India moved steadily northeastward at 70–80 mm/year during ca. 79–68 Ma and up to 180 mm/year at ca. 66–63 Ma. The reasons for this acceleration mainly resulted from the increased seafloor spreading in the southern and southwestern Indian Ocean (Conrad and Lithgow-Bertelloni, 2007) and the Reunion plume head spreading (van Hinsbergen et al., 2011). The subsequent rapid slowdown from ~180 mm/year at ca. 63 Ma to ~110 mm/year at ca. 61 Ma is synchronous with the final closure of the Neo-Tethyan Ocean and the continent-continent collision between the Tibetan Himalaya and Asia. India's motion temperately accelerated from ~110 mm/year at ca. 61 Ma to ~130 mm/year at ca. 53 Ma, which corresponds to the shrinkage of the North India Sea; subsequently, India's motion shows a notable slowdown to ~50 mm/year at ca. 47 Ma, which is fully consistent with the diachronous, west to east closure of the North India Sea.

4.4.2. Mantle tomography

The triple-stage India-Asia collision scenario is well documented by deep-mantle tomographic images, which display three major zones of relatively high P-wave velocities (Van der Voo et al., 1999), as shown in Fig. 7B. Firstly, the intra-oceanic subducted slab (Van der Voo et al., 1999; Aitchison et al., 2007) resulting from the collision of the Tibetan Himalaya with the TTSZ at ca. 64 Ma is represented by the southernmost deeper-mantle anomaly (labelled III in Fig. 7B). Secondly, the shallower anomaly (labelled II in Fig. 7B) is generally considered to represent the subducted Neo-Tethyan oceanic lithosphere (Van der Voo et al., 1999; van Hinsbergen et al., 2012), which broke off sometime after the collision of the Tibetan Himalaya terrane with the Lhasa terrane at ca. 61 Ma. Finally, we interpret the upper right anomaly (labelled I in Fig. 7B) to represent the subducted North-India-Sea oceanic lithosphere, which

resulted from the collision between India and the Tibetan Himalaya at ca. 53–47 Ma (Fig. 6D and E), and probably broke off at ca. 45 Ma. In addition, the size of the North India Sea (Fig. 6C) is consistent with the size of anomaly I (Fig. 8B) as the slab of the subducted North-India-Sea oceanic lithosphere represented in Fig. 4a–c of Van der Voo et al. (1999) is much larger in central vertical section than in western vertical section.

4.4.3. Continental deformation

The new collision history presented here consistently explains multiple lines of evidence from continental deformation. In the northwestern Himalaya, the Muslim Bagh, Bela, Zhob, Waziristan and Khost ophiolites obducted onto the Tibetan Himalaya during the late Cretaceous to early Paleocene (Beck et al., 1996; Khan et al., 2009). In western Pakistan, the youngest sedimentary rocks below the obducted ophiolites are of late Maastrichtian age (ca. 67 Ma), and the oldest sedimentary rocks unconformably overlying the ophiolites are of early Eocene age (ca. 50 Ma) (Khan et al., 2009). All these observations support the ca. 64-Ma-collision between the Tibetan Himalaya and the TTSZ.

In the eastern Lhasa terrane, the collision of the Tibetan Himalaya (plus the accreted TTSZ) with Asia at ca. 61 Ma produced a prominent large-scale regional unconformity between the Paleocene Dianzhong volcanic rocks (the lowest unit of the Linzizong Group) and the underlying Upper Cretaceous red sediments and rocks of the Shexing Formation (Mo et al., 2003).

The final continent-continent collision between India and the Tibetan Himalaya at ca. 53–47 Ma can account for a series of observations of continental deformation. For example, the Linzizong volcanic rocks in the southern Lhasa terrane and the coeval sedimentary rocks in the Xigaze forearc basin only experienced slight deformation (Yin and Harrison, 2000; Hu et al., 2016). The Gangdese arc also did not suffer significant compression during the Paleocene to early Eocene (Zhu et al., 2017). The Lagen La thrust and Sinongduo thrust systems in southern Tibet initiated in the early Eocene (Pullen et al., 2008; Yang et al., 2022), which indicates that crustal shortening and thickening occurred in the Lhasa terrane during that time. The Himalayan crustal thickening may have triggered high-grade metamorphism at ca. 44 Ma (Aikman et al., 2008).

4.4.4. Magmatism and ultra-high pressure metamorphism

The LA-ICP-MS zircon U-Pb geochronology of volcanic and plutonic

rocks of the Kohistan-Ladakh arc indicates *syn*-collisional calc-alkaline igneous activity at ca. 65–61 Ma (Khan et al., 2009). Furthermore, these arc igneous rocks yielded DUPAL source (Southern Hemisphere) isotopic signatures and the Kohistan-Ladakh arc developed on a northward-dipping subduction zone (Khan et al., 2009). These observations provide magmatic evidence supporting the ca. 64-Ma-collision between the Tibetan Himalaya and the TTSZ.

The Linzizong volcanic rocks, which formed between 64.43 Ma and 43.93 Ma and consists of the Dianzhong (64.43–60 Ma), Nianbo (54.07 Ma) and Pana (48.73–43.93 Ma) formations (Zhou et al., 2004), which recorded the syn-collisional to post-collisional magmatic processes during the continental collision between India and Asia (Mo et al., 2003). The Dianzhong Formation, consisting of andesitic lavas and pyroclastic deposits, was considered to result from syn-collisional magmatism (Mo et al., 2003; Mo et al., 2008). Thus, we suggest that the Dianzhong volcanic rocks represent the syn-collisional magmatic response to the ca. 61-Ma-collision between the Tibetan Himalaya (plus the accreted TTSZ) and Asia. The high potassium volcanic rocks of the Nianbo and Pana formations reflect environments of intra-continental convergence and crustal thickening (Mo et al., 2003; Mo et al., 2008); we thus suggest that the Nianbo and Pana volcanic rocks represent the post-collisional magmatic response to the 53–47-Ma-collision between India and the Tibetan Himalaya.

Additionally, the middle Eocene leucogranites in the Tethyan and Greater Himalayan sequences represent post-collisional magmatic products (e.g., Pullen et al., 2011; Hou et al., 2012; Huang et al., 2021); and we suggest that they were related to the break-off process of the North-India-Sea oceanic slab. Similarly, we suggest that the discovery of the OIB-type gabbro dated at ca. 45 Ma (SIMS U-Pb age of titanite) from the Tethyan Himalaya (Ji et al., 2016) further confirmed the break-off of the North-India-Sea oceanic slab during the middle Eocene. Consequently, we argue that the coeval presence of the Himalayan leucogranites (e.g., Pullen et al., 2011; Hou et al., 2012) and the OIB-type gabbro (Ji et al., 2016) were related to thermal perturbations caused by break-off of the southern North-India-Sea oceanic slab rather than the northern Neo-Tethyan oceanic slab. Moreover, the ultra-high pressure metamorphism in the western Himalaya occurred at ca. 53–47 Ma (e.g., Leech et al., 2005; Donaldson et al., 2013; Weller et al., 2021), which most likely resulted from the continent-continent collision between India and the Tibetan Himalaya at ca. 53–47 Ma.

4.4.5. Stratigraphy and sedimentology

4.4.5.1. Sediment provenance. Detrital zircon U-Pb geochronology can provide useful information signaling sediment provenance. The 61-Ma-collision between the Tibetan Himalaya (plus the accreted TTSZ) and Asia explains the appearance of Asian detritus at ca. 60 Ma (Wu et al., 2014; DeCelles et al., 2014; Hu et al., 2015; An et al., 2021).

Detrital zircon U-Pb geochronology data from the Himalayan orogenic belt support the continental collision between India and the Tibetan Himalaya at ca. 53–47 Ma. The northernmost sub-Himalaya terrane acquired grains derived from Asia at ca. 55 Ma (Ding et al., 2016) and deposition of Asian material in the lower Indus basin began at ca. 50 Ma (Zhuang et al., 2015); and from this time onwards, the provenance of this basin maintains consistency, with few variations (Zhuang et al., 2015). Detrital zircon U-Pb geochronology data and Hf isotopic analyses indicate that the Subathu Formation in the western part of the Lesser Himalaya in northwest India contains detritus originating from the Tethyan Himalaya, the Kohistan-Ladakh arc and Asia at no later than ca. 50–44 Ma (Colleps et al., 2020). The central part of the Lesser Himalaya acquired detritus originating from the Tethyan Himalaya prior ca. 45 Ma (DeCelles et al., 2004; Najman et al., 2005). The above-mentioned studies have lent strong support for the diachronous collision between India and Tibetan Himalaya at ca. 53–47 Ma.

4.4.5.2. Sedimentary basin deformation and sedimentation pattern. The ca. 53–47 Ma collision of India and the Tibetan Himalaya can account for the tectonic deformation recorded in the sedimentary basins of eastern Tibet, such as the ~30° clockwise rotation during ca. 52–48 Ma in the Gonjo Basin (Li et al., 2020a, 2020b), the ~25.9° counterclockwise rotation during ca. 52–46 Ma in the Nangqian Basin (Zhang et al., 2020), and the ~45° counterclockwise rotation during ca. 51–49 Ma in the Xialaxiu Basin (Cogné et al., 1999). The sediment accumulation rates significantly increased at ca. 52–48 Ma in the Gonjo Basin (Li et al., 2020a) and at ca. 54–52 Ma in the Hoh Xil Basin (Jin et al., 2018), north-central Tibet. After the continental collision at ca. 53–47 Ma, the ongoing convergence between India and Asia caused Himalayan uplift and associated erosional exhumation, which explains the absence of sedimentary rocks of Eocene-Oligocene age in the Himalayan orogenic belt (Yin, 2006; Hu et al., 2017). Additionally, the continental collision at ca. 53–47 Ma shaped the sedimentation pattern over the Bengal Basin, which is characterized by a rapid increase in the influx of detritus from the Himalayan orogenic belt in the middle Eocene (Alam et al., 2003).

4.4.5.3. Cessation of marine sedimentation. Rowley (1996) considered that the age of the youngest marine strata could represent the timing of the India-Asia collision onset. Then, he reviewed stratigraphic evidence from the Himalayan region and proposed that a diachronous collision occurred, starting in the late Ypresian (ca. 52 Ma) in the west, and gradually into the Lutetian (ca. 48–42 Ma) in the east.

Recent studies have established a west to east gradual cessation of shallow marine sedimentation in the Tethyan Himalaya, which occurred in the early Eocene in Zanskar, northwestern India (ca. 53–51 Ma; Najman et al., 2017), in the late Lutetian in the Tingri and Gamba areas, southern Tibet (ca. 43–41 Ma; Willems et al., 1996), and in the Priabonian in the Düela area, southern Tibet (ca. 35 Ma; Wang et al., 2020). These observations are all consistent with the diachronous closure of the North India Sea from west to east, which can be attributed to the final episode of continent-continent collision between India and the Tibetan Himalaya at ca. 53–47 Ma.

4.4.6. Faunal migration

The Vastan fauna in India documents the earliest record of immigration to the Indian subcontinent, which includes some possibly endemic (e.g., cambaytheriid perissodactyls) and several holarctic or northern families of mammals (adapoid, omomyid, and eosimiid primates; dichobunid artiodactyls; and ailuravine rodents) (e.g., Clementz et al., 2011). Clementz et al. (2011) presented new and independent data from microfossil biostratigraphy, mammal fossils, strontium and carbon isotopes from a lower Eocene marine sequence at the Vastan Lignite Mine of western India. The results provide solid evidence for terrestrial faunal exchanges between Asia and India before 53.7 Ma. Moreover, the Ghazij Formation in Pakistan also contained the modern orders of mammals (artiodactyls, perissodactyls, primates) on the Indian subcontinent at ca. 53.3–50.0 Ma (Clyde et al., 2003). These two pieces of evidence are well in line with the final continental collision between India and the Tibetan Himalaya at ca. 53–47 Ma.

4.5. Implications for paleogeography and paleoenvironment

Our proposed triple-stage India-Asia collision scenario provides accurate constraints on the latitudinal distribution of Neo-Tethyan landmasses (i.e. India, Tethyan Himalaya and Tibetan Himalaya), and the size of Neo-Tethyan ocean basins (i.e. Neo-Tethys Ocean and North India Sea) during the late Cretaceous to early Cenozoic (ca. 75–50 Ma). The Tethyan Himalaya was situated at paleolatitudes of ~19.4°S at ca. 75 Ma (Yuan et al., 2021) and ~ 14.1°N at ca. 61 Ma, respectively. This suggests that at ca. 75 Ma the Tethyan Himalaya terrane was separated from the Lhasa terrane by the equatorial Neo-Tethys Ocean, which had a north-south width of ~33°, equivalent to ~3600 km (Fig. 6A). After ca.

75 Ma the Tibetan Himalaya terrane rifted away from India and collided with the Lhasa terrane at ca. 61 Ma. The rifting during ca. 75 Ma to ca. 61 Ma generated an equatorial North India Sea, which had a north-south width of ~2200 km at its central part and ~ 1300 km at its western part (Fig. 6B, C). The North India Sea diachronously closed at ca. 53–47 Ma from west to east due to the collision of Tibetan Himalaya terrane and India.

The long-standing presence of equatorial ocean basins (i.e. the Neo-Tethys Ocean and North India Sea) during ca. 75 Ma to ca. 50 Ma between Asia and India may have played an important role in maintaining poleward heat and moisture transport, thus contributing to the warm climate conditions during the late Cretaceous to early Eocene climate optimum. Subsequently, the continental collision of India with the Tibetan Himalaya terrane and associated closure of the North India Sea during the early to middle Eocene (Fig. 7) marks the final amalgamation of India and Asia, thus forming the Eurasian continent. The ensued major changes in the Asian land-sea distribution pattern (e.g. Palcu and Krijgsman, 2022), together with the uplift of the Himalayan-Tibetan complex and the retreat of the proto-Paratethys Sea (Ramstein et al., 1997; Kaya et al., 2019) during the ongoing convergence between India and Asia may have triggered the transition from planetary subtropical aridity patterns to inland aridity patterns during the late Paleogene (Guo et al., 2008; Guo, 2017; Fan et al., 2020). In addition, the reach of the highly weatherable Deccan Traps in southwestern India to the equatorial humid belt at around 50 Ma, roughly contemporaneous with the closure of the North India Sea, has led to the consumption of large amounts of CO_2 since the early Eocene climate optimum at ca. 50 Ma, thus significantly contributing to lowering atmospheric CO_2 concentrations and resulting global cooling (Kent and Muttoni, 2008; Kent and Muttoni, 2013). These combined effects may have led to a major reorganization of Asian paleoenvironment pattern during the late Paleogene (Guo et al., 2008; Guo, 2017; Fang et al., 2021; Zheng et al., 2022) and ultimately formed the present monsoon-arid environment pattern during the terminal Oligocene to early Miocene in Central-Eastern Asia (Guo et al., 2002; Guo et al., 2008; Guo, 2017).

5. Conclusions

We have presented new paleomagnetic data from the red siliceous shales and cherts of the mid-Paleocene Sangdanlin Formation in the distal northern part of the Tethyan Himalaya terrane. Paleomagnetic and rock magnetic analyses reveal that these rocks contain a secondary magnetic signal carried by authigenic hematite and a primary magnetic signal of dual polarities carried by detrital hematite. The combined evidence of our new and previously published (Yuan et al., 2021) paleomagnetic data constrains the location of the Tethyan Himalaya to a paleolatitude of $14.1° ± 1.9°N$ at ca. 61 Ma, overlapping with that of the southern margin of the Asian continent (Lhasa terrane).

With the addition of recently published high-quality paleomagnetic data of the Kohistan-Ladakh arc in Ladakh, India (Martin et al., 2020), we suggest that the India-Asia collision represents a triple-stage collision process, firstly the arc-continent collision between the Tibetan Himalaya and the TTSZ occurring at a paleolatitude of ~8.1°N at ca. 64 Ma, subsequently the continental collision between the Tibetan Himalaya (plus the accreted TTSZ) and Lhasa terranes occurring at a paleolatitude of ~14°N at ca. 61 Ma, and finally the continental collision between India and the Tibetan Himalaya at ca. 53–47 Ma, diachronously closing the North India Sea from west to east.

The triple-stage collision scenario well accounts for the variations of convergence rates between India and Asia, and is convincingly documented by seismic tomographic images indicative of the presence of three slab remnants below Tibet and India. In addition, this scenario reconciles multiple lines of evidence from geology, geochemistry and paleontology for the India-Asia collision.

Declaration of Competing Interest

The authors declare that they have no competing financial interests or personal relationships that could have influenced the work reported in this paper.

Appendix A. Supplementary data

Supplementary data to this article can be found online at https://doi.org/10.1016/j.gloplacha.2022.103821.

References

Agnini, C., Fornaciari, E., Raffi, I., Catanzariti, R., Pälike, H., Backman, J., Rio, D., 2014. Biozonation and biochronology of Paleogene calcareous nannofossils from low and middle latitudes. Newsl. Stratigr. 47, 131–181. https://doi.org/10.1127/0078-0421/2014/0042.

Aikman, A.B., Harrison, T.M., Ding, L., 2008. Evidence for early (>44 Ma) Himalayan crustal thickening, Tethyan Himalaya, southeastern Tibet. Earth Planet. Sci. Lett. 274, 14–23. https://doi.org/10.1016/j.epsl.2008.06.038.

Aitchison, J.C., Badengzhu, Davis, A.M., Liu, J., Luo, H., Malpas, J., McDermid, I.M.C., Wu, H., Ziabrev, S., Zhou, M.F., 2000. Remnants of a cretaceous intra-oceanic subduction system within the Yarlung-Zangbo suture (southern Tibet). Earth Planet. Sci. Lett. 183, 231–244. https://doi.org/10.1016/S0012-821X(00)00287-9.

Aitchison, J.C., Ali, J.R., Davis, A.M., 2007. When and where did India and Asia collide? J. Geophys. Res. 112, B05423 https://doi.org/10.1029/2006JB004706.

Alam, M., Alam, M.M., Curray, J.R., Chowdhury, M.L.R., Gani, M.R., 2003. An overview of the sedimentary geology of the Bengal Basin in relation to the regional tectonic framework and basin-fill history. Sediment. Geol. 155, 179–208. https://doi.org/10.1016/S0037-0738(02)00180-X.

Ali, J.R., Aitchison, J.C., 2005. Greater india. Earth-Sci. Rev. 72, 169–188. https://doi.org/10.1016/j.earscirev.2005.07.005.

Allègre, C.J., Courtillot, V., Tapponnier, P., Hirn, A., Mattauer, M., Coulon, C., Jaeger, J. J., Achache, J., Schärer, U., Marcoux, J., Burg, J.P., Girardeau, J., Armijo, R., Gariépy, C., Göper, C., Li, T., Xiao, X., Chang, C., Li, G., Lin, B., Teng, J., Wang, N., Chen, G., Han, T., Wang, X., Den, W., Sheng, H., Cao, Y., Zhou, J., Qiu, H., Bao, P., Wang, S., Wang, B., Zhou, Y., Xu, R., 1984. Structure and evolution of the Himalaya-Tibet orogenic belt. Nature 307, 17–22. https://doi.org/10.1038/307017a0.

An, W., Hu, X., Garzanti, E., Wang, J.G., Liu, Q., 2021. New precise dating of the India-Asia collision in the Tibetan Himalaya at 61 Ma. Geophys. Res. Lett. 48, e2020GL090641 https://doi.org/10.1029/2020GL090641.

Argand, E., 1924. La tectonique de l' Asie. In: Proc. 13th Int. Geol. Cong., vol. 7, pp. 181–372.

Beck, R.A., Burbank, D.W., Sercombe, W.J., Khan, A.M., Lawrence, R.D., 1996. Late cretaceous ophiolite obduction and Paleocene India-Asia collision in the westernmost Himalaya. Geodin. Acta 9, 114–144. https://doi.org/10.1080/09853111.1996.11105281.

Bian, W., Yang, T., Ma, Y., Jin, J., Gao, F., Wang, S., Peng, W., Zhang, S., Wu, H., Li, H., Cao, L., 2019. Paleomagnetic and geochronological results from the Zhela and Weimei Formations lava flows of the eastern Tethyan Himalaya: new insights into the breakup of eastern Gondwana. J. Geophys. Res. Solid Earth 124, 44–64. https://doi.org/10.1029/2018JB016403.

Brown, B., Müller, R.D., Struckmeyer, H.I.M., Gaina, C., Stagg, H., Symonds, P., 2003. Formation and evolution of Australian passive margins: implications for locating the boundary between continental and oceanic crust. In: Hillis, R.R., Müller, R.D. (Eds.), Evolution and Dynamics of the Australian Plate, vol. 372, pp. 223–243. https://doi.org/10.1130/0-8137-2372-8.223. Spec. Publ. Geol. Soc. Aust. No. 22 and Spec. Pap. Geol. Soc. Am.

Burbank, D.W., Beck, R.A., Mulder, T., 1997. The Himalayan foreland basin. In: Yin, A., Harrison, M. (Eds.), The Tectonic Evolution of Asia. Cambridge University Press, Cambridge.

Cande, S.C., Stegman, D.R., 2011. Indian and African plate motions driven by the push force of the Réunion plume head. Nature 475, 47–52. https://doi.org/10.1038/nature10174.

Clementz, M., Bajpai, S., Ravikant, V., Thewissen, J.G.M., Saravanan, N., Singh, I.B., Prasad, V., 2011. Early Eocene warming events and the timing of terrestrial faunal exchange between India and Asia. Geology 39, 15–18. https://doi.org/10.1130/G31585.1.

Clift, P.D., Hodge, K.V., Heslop, D., Hannigan, R., Hoang, V.L., Calves, G., 2008. Correlation of Himalayan exhumation rates and Asian monsoon intensity. Nat. Geosci. 1, 875–880. https://doi.org/10.1038/ngeo351.

Clyde, W.C., Khan, I.H., Gingerich, P.D., 2003. Stratigraphic response and mammalian dispersal during initial India-Asia collision: evidence from the Ghazij Formation, Balochistan, Pakistan. Geology 31, 1097–1100. https://doi.org/10.1130/G19956.1.

Cogné, J.P., Halim, N., Chen, Y., Courtillot, V., 1999. Resolving the problem of shallow magnetizations of tertiary age in Asia: insights from paleomagnetic data from the Qiangtang, Kunlun, and Qaidam blocks (Tibet, China), and a new hypothesis. J. Geophys. Res. 104, 17715–17734. https://doi.org/10.1029/1999JB900153.

Coleman, M.E., 1996. Orogen-parallel and orogen-perpendicular extension in the central Nepalese Himalayas. Geol. Soc. Am. Bull. 108, 1594–1607. https://doi.org/10.1130/0016-7606(1996)108<1594:OPAOPE>2.3.CO;2.

Colleps, C.L., McKenzie, N.R., Horton, B.K., Webb, A.A.G., Ng, Y.W., Singh, B.P., 2020. Sediment provenance of pre-and post-collisional Cretaceous–Paleogene strata from the frontal Himalaya of northwest India. Earth Planet. Sci. Lett. 534, 116079 https://doi.org/10.1016/j.epsl.2020.116079.

Conrad, C.P., Lithgow-Bertelloni, C., 2007. Faster seafloor spreading and lithosphere production during the mid-Cenozoic. Geology 35, 29–32. https://doi.org/10.1130/G22759A.1.

Critelli, S., Garzanti, E., 1994. Provenance of the lower Tertiary Murree redbeds (Hazara-Kashmir Syntaxis, Pakistan) and initial rising of the Himalayas. Sediment. Geol. 89, 265–284. https://doi.org/10.1016/0037-0738(94)90097-3.

Dannemann, S., Appel, E., Rösler, W., Neumann, U., Liebke, U., Nag, D., 2022. Paleomagnetic indication for India-Asia collision at 12°N and maximum 810 km Greater India extent in the western suture zone. Geophys. J. Int. 229, 1193–1211. https://doi.org/10.1093/gji/ggab528.

DeCelles, P.G., Gehrels, G.E., Quade, J., Ojha, T.P., Kapp, P.A., Upreti, B.N., 1998. Neogene foreland deposits, erosional unroofing, and the kinematic history of the Himalayan fold-thrust belt, western Nepal. Geol. Soc. Am. Bull. 110, 2–21. https://doi.org/10.1130/0016-7606(1998)110<0002:NFBDEU>2.3.CO;2.

DeCelles, P.G., Robinson, D.M., Zandt, G., 2002. Implications of shortening in the Himalayan fold-thrust belt for uplift of the Tibetan Plateau. Tectonics 21, 1062. https://doi.org/10.1029/2001TC001322.

DeCelles, P.G., Gehrels, G.E., Najman, Y., Martin, A.J., Carter, A., Garzanti, E., 2004. Detrital geochronology and geochemistry of Cretaceous–Early Miocene strata of Nepal: implications for timing and diachroneity of initial Himalayan orogenesis. Earth Planet. Sci. Lett. 227, 313–330. https://doi.org/10.1016/j.epsl.2004.08.019.

DeCelles, P.G., Kapp, P., Gehrels, G.E., Ding, L., 2014. Paleocene–Eocene foreland basin evolution in the Himalaya of southern Tibet and Nepal: implications for the age of initial India-Asia collision. Tectonics 33, 824–849. https://doi.org/10.1002/2014TC003522.

Deng, C.L., He, H.Y., Pan, Y.X., Zhu, R.X., 2013. Chronology of the terrestrial Upper Cretaceous in the Songliao Basin, northeast Asia. Palaeogeogr. Palaeoclimatol. Palaeoecol. 385, 44–54. https://doi.org/10.1016/j.palaeo.2012.07.028.

Ding, L., Kapp, P., Wan, X., 2005. Paleocene–Eocene record of ophiolite obduction and initial India-Asia collision, south central Tibet. Tectonics 24, TC3001. https://doi.org/10.1029/2004TC001729.

Ding, L., Qasim, M., Jadoon, I.A., Khan, M.A., Xu, Q., Cai, F., Wang, H., Baral, U., Yue, Y., 2016. The India–Asia collision in north Pakistan: insight from the U–Pb detrital zircon provenance of Cenozoic foreland basin. Earth Planet. Sci. Lett. 455, 49–61. https://doi.org/10.1016/j.epsl.2016.09.003.

Ding, L., Maksatbek, S., Cai, F., Wang, H., Song, P., Ji, W., Xu, Q., Zhang, L., Muhammad, Q., Upendra, B., 2017. Processes of initial collision and suturing between India and Asia. Sci. China Earth Sci. 60, 635–651. https://doi.org/10.1007/s11430-016-5244-x.

Ding, W.N., Ree, R.H., Spicer, R.A., Xing, Y.W., 2020. Ancient orogenic and monsoon-driven assembly of the world's richest temperate alpine flora. Science 369, 578–581. https://doi.org/10.1126/science.abb4484.

Donaldson, D.G., Webb, A.A.G., Menold, C.A., Kylander-Clark, A.R.C., Hacker, B.R., 2013. Petrochronology of Himalayan ultrahigh-pressure eclogite. Geology 41, 835–838. https://doi.org/10.1130/G33699.1.

Fan, M., Feng, R., Geissman, J.W., Poulsen, C.J., 2020. Late Paleogene emergence of a north American loess plateau. Geology 48, 273–277. https://doi.org/10.1130/G47102.1.

Fang, X., Yan, M., Zhang, W., Nie, J., Han, W., Wu, F., Song, C., Zhang, T., Zan, J., Yang, Y., 2021. Paleogeography control of Indian monsoon intensification and expansion at 41 Ma. Sci. Bull. 66, 2320–2328. https://doi.org/10.1016/j.scib.2021.07.023.

Fielding, E., Isacks, B., Barazangi, M., Duncan, C., 1994. How flat is Tibet? Geology 22, 163–167. https://doi.org/10.1130/0091-7613(1994)022<0163:HFIT>2.3.CO;2.

Fisher, R.A., 1953. Dispersion on a sphere. Proc. R. Soc. Lond. 217, 295–305. https://doi.org/10.1098/rspa.1953.0064.

Gansser, A., 1964. Geology of the Himalayas. Wiley, London.

Gao, R., Lu, Z., Klemperer, S.L., Wang, H., Dong, S., Li, W., Li, H., 2016. Crustal-scale duplexing beneath the Yarlung Zangbo suture in the western Himalaya. Nat. Geosci. 9, 555–560. https://doi.org/10.1038/NGEO2730.

Garzanti, E., Baud, A., Mascle, G., 1987. Sedimentary record of the northward flight of India and its collision with Eurasia (Ladakh Himalaya, India). Geodin. Acta 1, 297–312. https://doi.org/10.1080/09853111.1987.11105147.

Gibbons, A.D., Barckhausen, U., van den Bogaard, P., Hoernle, K., Werner, R., Whittaker, J.M., Müller, R.D., 2012. Constraining the Jurassic extent of Greater India: tectonic evolution of the West Australian margin. Geochem. Geophys. Geosyst. 13, Q05W13 https://doi.org/10.1029/2011GC003919.

Gradstein, F.M., Ogg, J.G., Schmitz, M.D., Ogg, G.M., 2020. The Geologic Time Scale 2020. Elsevier, Amsterdam.

Guo, Z.T., 2017. Loess Plateau attests to the onsets of monsoon and deserts (in Chinese). Sci. Sin. Terrae 47, 421–437. https://doi.org/10.1360/N072017-00037.

Guo, Z.T., Ruddiman, W.F., Hao, Q.Z., Wu, H.B., Qiao, Y.S., Zhu, R.X., Peng, S.Z., Wei, J.J., Yuan, B.Y., Liu, T.S., 2002. Onset of Asian desertification by 22 Myr ago inferred from loess deposits in China. Nature 416, 159–163. https://doi.org/10.1038/416159a.

Guo, Z.T., Sun, B., Zhang, Z.S., Peng, S.Z., Xiao, G.Q., Ge, J.Y., Hao, Q.Z., Qiao, Y.S., Liang, M.Y., Liu, J.F., Yin, Q.Z., Wei, J.J., 2008. A major reorganization of Asian climate by the early Miocene. Clim. Past 4, 153–174. https://doi.org/10.5194/cp-4-153-2008.

Hall, R., 2012. Late Jurassic-Cenozoic reconstructions of the Indonesian region and the Indian Ocean. Tectonophysics 570, 1–41. https://doi.org/10.1016/j.tecto.2012.04.021.

van Hinsbergen, D.J.J., Schouten, T.L.A., 2021. Deciphering paleogeography from orogenic architecture: constructing orogens in a future supercontinent as thought experiment. Am. J. Sci. 321, 955–1031. https://doi.org/10.2475/06.2021.09.

van Hinsbergen, D.J.J., Steinberger, B., Doubrovine, P.V., Gassmöller, R., 2011. Acceleration and deceleration of India-Asia convergence since the Cretaceous: Roles of mantle plumes and continental collision. J. Geophys. Res. 116, B06101 https://doi.org/10.1029/2010JB008051.

van Hinsbergen, D.J.J., Lippert, P.C., Dupont-Nivet, G., McQuarrieh, N., Doubrovine, P.V., Spakman, W., Torsvik, T.H., 2012. Greater India Basin hypothesis and a two-stage Cenozoic collision between India and Asia. Proc. Natl. Acad. Sci. U. S. A. 109, 7659–7664. https://doi.org/10.1073/pnas.1117262109.

van Hinsbergen, D.J.J., Lippert, P.C., Li, S., Huang, W., Advokaat, E.L., Spakman, W., 2019. Reconstructing Greater India: paleogeographic, kinematic, and geodynamic perspectives. Tectonophysics 760, 69–94. https://doi.org/10.1016/j.tecto.2018.04.006.

Hodges, K.V., 2000. Tectonics of the Himalaya and southern Tibet from two perspectives. Geol. Soc. Am. Bull. 112, 324–350. https://doi.org/10.1130/0016-7606(2000)112<324:TOTHAS>2.0.CO;2.

Hodges, K.V., Parrish, R.R., Searle, M.P., 1996. Tectonic evolution of the Central Annapurna Range, Nepalese Himalayas. Tectonics 15, 1264–1291. https://doi.org/10.1029/96TC01791.

Hodych, J.P., Buchan, K.L., 1994. Early Silurian Palaeolatitude of the Springdale Group redbeds of Central Newfoundland: a palaeomagnetic determination with a remanence anisotropy test for inclination error. Geophys. J. Int. 117, 640–652. https://doi.org/10.1111/j.1365-246X.1994.tb02459.x.

Hou, Z.Q., Zheng, Y.C., Zeng, L.S., Gao, L.E., Huang, K.X., Li, W., Li, Q.Y., Fu, Q., Liang, W., Sun, Q.Z., 2012. Eocene-Oligocene granitoids in southern Tibet: constraints on crustal anatexis and tectonic evolution of the Himalayan orogen. Earth Planet. Sci. Lett. 349-350, 38–52. https://doi.org/10.1016/j.epsl.2012.06.030.

Hu, X., Garzanti, E., Moore, T., Raffi, I., 2015. Direct stratigraphic dating of India-Asia collision onset at the Selandian (middle Paleocene, 59 ± 1 Ma). Geology 43, 859–862. https://doi.org/10.1130/G36872.1.

Hu, X., Wang, J.G., BouDagher-Fadel, M., Garzanti, E., An, W., 2016. New insights into the timing of the India-Asia collision from the Paleogene Quxia and Jialazi formations of the Xigaze forearc basin, South Tibet. Gondwana Res. 32, 76–92. https://doi.org/10.1016/j.gr.2015.02.007.

Hu, X., Wang, J., An, W., Garzanti, E., Li, J., 2017. Constraining the timing of the India-Asia continental collision by the sedimentary record. Sci. China Earth Sci. 60, 603–625. https://doi.org/10.1007/s11430-016-9003-6.

Huang, F., Bai, R., Deng, G., Liu, X., Li, X., 2021. Barium isotope evidence for the role of magmatic fluids in the origin of Himalayan leucogranites. Sci. Bull. 66, 2329–2336. https://doi.org/10.1016/j.scib.2021.07.020.

Huang, W., van Hinsbergen, D.J.J., Dekkers, M.J., Garzanti, E., Dupont-Nivet, G., Lippert, P.C., Li, X., Maffione, M., Langereis, C.G., Hu, X., Guo, Z., Kapp, P., 2015. Paleolatitudes of the Tibetan Himalaya from primary and secondary magneti-zations of Jurassic to Lower Cretaceous sedimentary rocks. Geochem. Geophys. Geosyst. 16, 77–100. https://doi.org/10.1002/2014GC005624.

Ingalls, M., Rowley, D.B., Currie, B., Colman, A.S., 2016. Large-scale subduction of continental crust implied by India-Asia mass-balance calculation. Nat. Geosci. 9, 848–853. https://doi.org/10.1038/NGEO2806.

Jadoon, U.F., Huang, B., Shah, S.A., Rahim, Y., Khan, A.A., Bibi, A., 2022. Multi-stage India-Asia collision: paleomagnetic constraints from Hazara-Kashmir syntaxis in the western Himalaya. Geol. Soc. Am. Bull. https://doi.org/10.1130/B36116.1 (In press).

Jagoutz, O., Royden, L., Holt, A.F., Becker, T.W., 2015. Anomalously fast convergence of India and Eurasia caused by double subduction. Nat. Geosci. 8, 475–478. https://doi.org/10.1038/ngeo2418.

Ji, W.Q., Wu, F.Y., Chung, S.L., Wang, X.C., Liu, C.Z., Li, Q.L., Liu, Z.C., Liu, X.C., Wang, J.G., 2016. Eocene Neo-Tethyan slab breakoff constrained by 45 Ma oceanic island basalt-type magmatism in southern Tibet. Geology 44, 283–286. https://doi.org/10.1130/G37612.1.

Jiang, Z., Liu, Q., Dekker, M.J., Zhao, X., Roberts, A.P., Yang, Z., Jin, C., Liu, J., 2017. Remagnetization mechanisms in Triassic red beds from South China. Earth Planet. Sci. Lett. 479, 219–230. https://doi.org/10.1016/j.epsl.2017.09.019.

Jiang, Z., Liu, Q., Roberts, A.P., Dekkers, M.J., Barrón, V., Torrent, J., Li, S., 2022. The magnetic and color reflectance properties of hematite: from Earth to Mars. Rev. Geophys. 60, e2020RG000698 https://doi.org/10.1029/2020RG000698.

Jin, C., Liu, Q., Liang, W., Roberts, A.P., Sun, J., Hu, P., Zhao, X., Su, Y., Jiang, Z., Liu, Z., Duan, Z., Yang, H., Yuan, G., 2018. Magnetostratigraphy of the Fenghuoshan Group in the Hoh Xil Basin and its tectonic implications for India–Eurasia collision and Tibetan Plateau deformation. Earth Planet. Sci. Lett. 486, 41–53. https://doi.org/10.1016/j.epsl.2018.01.010.

Kapp, P., DeCelles, P.G., 2019. Mesozoic–Cenozoic geological evolution of the Himalayan-Tibetan orogen and working tectonic hypotheses. Am. J. Sci. 319, 159–254. https://doi.org/10.2475/03.2019.01.

Kaya, M.Y., Dupont-Nivet, G., Proust, J.N., Roperch, P., Bougeois, L., Meijer, N., Frieling, J., Fioroni, C., Özkan Altıner, S., Vardar, E., Barbolini, N., Stoica, M., Aminov, J., Mamtimin, M., Zhaojie, G., 2019. Paleogene evolution and demise of the proto-Parathys Sea in Central Asia (Tarim and Tajik basins): role of intensified tectonic activity at ca. 41 Ma. Basin Res. 31, 461–486. https://doi.org/10.1111/bre.12330.

Kent, D.V., Muttoni, G., 2013. Modulation of Late Cretaceous and Cenozoic climate by variable drawdown of atmospheric $pCO2$ from weathering of basaltic provinces on continents drifting through the equatorial humid belt. Clim. Past 9, 525–546. https://doi.org/10.5194/cp-9-525-2013.

Khan, S.D., Walker, D.J., Hall, S.A., Burke, K.C., Shah, M.T., Stockli, L., 2009. Did the Kohistan-Ladakh island arc collide first with India? Geol. Soc. Am. Bull. 121, 366–384. https://doi.org/10.1130/B26348.1.

Kirschvink, J.L., 1980. The least-squares line and plane and the analysis of palaeomagnetic data. Geophys. J. Int. 62, 699–718. https://doi.org/10.1111/j.1365-246X.1980.tb02601.x.

Klootwijk, C.T., Bingham, D.K., 1980. The extent of greater India, III. Palaeomagnetic data from the Tibetan Sedimentary series, Thakkhola region, Nepal Himalaya. Earth Planet. Sci. Lett. 51, 381–405. https://doi.org/10.1016/0012-821X(80)90219-8.

Kruiver, P.P., Dekkers, M.J., Heslop, D., 2001. Quantification of magnetic coercivity components by the analysis of acquisition curves of isothermal remanent magnetisation. Earth Planet. Sci. Lett. 189, 269–276. https://doi.org/10.1016/S0012-821X(01)00367-3.

Kumar, P., Yuan, X., Kumar, M.R., Kind, R., Li, X., Chadha, R.K., 2007. The rapid drift of the Indian tectonic plate. Nature 449, 894–897. https://doi.org/10.1038/nature06214.

Le Fort, P., 1975. Himalayas: the collided range. Present knowledge of the continental arc. Am. J. Sci. 275, 1–44.

Leech, M.L., Singh, S., Jain, A.K., Klemperer, S.L., Manickavasagam, R.M., 2005. The onset of India-Asia continental collision: early, steep subduction required by the timing of UHP metamorphism in the western Himalaya. Earth Planet. Sci. Lett. 234, 83–97. https://doi.org/10.1016/j.epsl.2005.02.038.

Li, S., van Hinsbergen, D.J.J., Najman, Y., Liu-Zeng, J., Deng, C., Zhu, R., 2020a. Does pulsed Tibetan deformation correlate with Indian plate motion changes? Earth Planet. Sci. Lett. 536, 116144 https://doi.org/10.1016/j.epsl.2020.116144.

Li, S., van Hinsbergen, D.J.J., Shen, Z., Najman, Y., Deng, C., Zhu, R., 2020b. Anisotropy of magnetic susceptibility (AMS) analysis of the Gonjo Basin as an independent constraint to date Tibetan shortening pulses. Geophys. Res. Lett. 47, e2020GL087531 https://doi.org/10.1029/2020GL087531.

Liu, L., Liu, L., Xu, Y.G., 2021. Intermittent post-Paleocene continental collision in South Asia. Geophys. Res. Lett. 48, e2021GL094531 https://doi.org/10.1029/2021GL094531.

Long, S.P., McQuarrie, N., Tobgay, T., Grujic, D., 2011. Geometry and crustal shortening of the Himalayan fold-thrust belt, eastern and Central Bhutan. Geol. Soc. Am. Bull. 123, 1427–1447. https://doi.org/10.1130/B30203.1.

Lowrie, W., 1990. Identification of ferromagnetic minerals in a rock by coercivity and unblocking temperature properties. Geophys. Res. Lett. 17, 159–162. https://doi.org/10.1029/GL017i002p00159.

Ma, Y., Yang, T., Bian, W., Jin, J., Zhang, S., Wu, H., Li, H., 2016. Early Cretaceous paleomagnetic and geochronologic results from the Tethyan Himalaya: Insights into the Neotethyan paleogeography and the India-Asia collision. Sci. Rep. 6, 21605. https://doi.org/10.1038/srep21605.

Martin, A.J., 2017. A review of Himalayan stratigraphy, magmatism, and structure. Gondwana Res. 49, 42–80. https://doi.org/10.1016/j.gr.2017.04.031.

Martin, C.R., Jagoutz, O., Upadhyay, R., Royden, L.H., Eddy, M.P., Bailey, E., Nichols, C.I.O., Weiss, B.P., 2020. Paleocene latitude of the Kohistan–Ladakh arc indicates multistage India-Eurasia collision. Proc. Natl. Acad. Sci. U. S. A. 117, 29487–29494. https://doi.org/10.1073/pnas.2009039117.

Matsuda, T., Isozaki, Y., 1991. Well-documented travel history of Mesozoic pelagic chert in Japan: from remote ocean to subduction zone. Tectonics 10, 475–499. https://doi.org/10.1029/90TC02134.

McElhinny, M.W., 1964. Statistical significance of the fold test in paleomagnetism. Geophys. J. R. Astron. Soc. 8, 338–340. https://doi.org/10.1111/j.1365-246X.1964.tb06300.x.

McFadden, P.L., 1990. A new fold test for paleomagnetic studies. Geophys. J. Int. 103, 163–169. https://doi.org/10.1111/j.1365-246X.1990.tb01761.x.

McFadden, P.L., McElhinny, M.W., 1990. Classification of the reversal test in palaeomagnetism. Geophys. J. Int. 103, 725–729. https://doi.org/10.1111/j.1365-246X.1990.tb05683.x.

Meng, J., Gilder, S.A., Wang, C., Coe, R.S., Tan, X., Zhao, X., He, K., 2019. Defining the Limits of Greater India. Geophys. Res. Lett. 46, 4182–4191. https://doi.org/10.1029/2019GL082119.

Misra, S., Froelich, P.N., 2012. Lithium isotope history of Cenozoic seawater: changes in silicate weathering and reverse weathering. Science 335, 818–823. https://doi.org/10.1126/science.1214697.

Mo, X., Niu, Y., Dong, G., Zhao, Z., Hou, Z., Zhou, S., Ke, S., 2008. Contribution of syncollisional felsic magmatism to continental crust growth: a case study of the Paleogene Linzizong volcanic Succession in southern Tibet. Chem. Geol. 250, 49–67. https://doi.org/10.1016/j.chemgeo.2008.02.003.

Mo, X.X., Zhao, Z.D., Deng, J.F., Dong, G.C., Zhou, S., Guo, T.Y., Zhang, S.Q., Wang, L.L., 2003. Response of volcanism to the India-Asia collision (in Chinese). Geosci. Front. 10, 135–148. https://doi.org/10.3321/j.issn:1005-2321.2003.03.013.

Molnar, P., Tapponnier, P., 1975. Cenozoic tectonics of Asia: effects of a continental collision. Science 189, 419–426. https://doi.org/10.1126/science.189.4201.419.

Kent, D.V., Muttoni, G., 2008. Equatorial convergence of India and early Cenozoic climate trends. Proc. Natl. Acad. Sci. U. S. A. 105, 16065–16070. https://doi.org/10.1073/pnas.0805382105.

Najman, Y., Carter, A., Oliver, G., Garzanti, E., 2005. Provenance of Eocene foreland basin sediments, Nepal: constraints to the timing and diachroneity of early Himalayan orogenesis. Geology 33, 309–312. https://doi.org/10.1130/G21161.1.

Najman, Y., Jenks, D., Godin, L., Boudagher-Fadel, M., Millar, I., Garzanti, E., Horstwood, M., Bracciali, L., 2017. The Tethyan Himalayan detrital record shows that India-Asia terminal collision occurred by 54 Ma in the Western Himalaya. Earth Planet. Sci. Lett. 459, 301–310. https://doi.org/10.1016/j.epsl.2016.11.036.

Palcu, D.V., Krijgsman, W., 2022. The dire straits of Parathys: Gateways to the anoxic giant of Eurasia. In: Straits and Seaways: Controls, Processes and Implications in Modern and Ancient Systems. Geol. Soc. London, Spec. Publ. SP523. https://doi.org/10.1144/SP523-2021-73 (in press).

Parsons, A.J., Hosseini, K., Palin, R.M., Sigloch, K., 2020. Geological, geophysical and plate kinematic constraints for models of the India-Asia collision and the post-Triassic central Tethys oceans. Earth-Sci. Rev. 202, 103084 https://doi.org/10.1016/j.earscirev.2020.103084.

Patzelt, A., Li, H., Wang, J., Appel, E., 1996. Palaeomagnetism of Cretaceous to Tertiary sediments from southern Tibet: evidence for the extent of the northern margin of India prior to the collision with Eurasia. Tectonophysics 259, 259–284. https://doi.org/10.1016/0040-1951(95)00181-6.

Paul, J., Ghosh, A., 2022. Could the Réunion plume have thinned the Indian craton? Geology 50, 346–350. https://doi.org/10.1130/G49492.1.

Powell, C.M., Roots, S.R., Veevers, J.J., 1988. Pre-breakup continental extension in eastern Gondwanaland and the early opening of the eastern Indian Ocean. Tectonophysics 155, 261–283. https://doi.org/10.1016/0040-1951(88)90269-7.

Pullen, A., Kapp, P., Gehrels, G.E., DeCelles, P.G., Brown, E.H., Fabijanic, J.M., Ding, L., 2008. Gangdese retroarc thrust belt and foreland basin deposits in the Damxung area, southern Tibet. J. Asian Earth Sci. 33, 323–336. https://doi.org/10.1016/j.jseaes.2008.01.005.

Pullen, A., Kapp, P., DeCelles, P.G., Gehrels, G.E., Ding, L., 2011. Cenozoic anatexis and exhumation of Tethyan Sequence rocks in the Xiao Gurla Range, Southwest Tibet. Tectonophysics 501, 28–40. https://doi.org/10.1016/j.tecto.2011.01.008.

Pusok, A.E., Stegman, D.R., 2020. The convergence history of India-Eurasia records multiple subduction dynamics processes. Sci. Adv. 6, eaaz8681 https://doi.org/10.1126/sciadv.aaz8681.

Qin, H., Zhao, X., Liu, S., Paterson, G.A., Jiang, Z., Cai, S., Li, J., Liu, Q., Zhu, R., 2020. An ultra-low magnetic field thermal demagnetizer for high-precision paleomagnetism. Earth Planets Space 72, 170. https://doi.org/10.1186/s40623-020-01304-0.

Qin, S.X., Li, Y.X., Li, X.H., Xu, B., Luo, H., 2019. Paleomagnetic results of Cretaceous cherts from Zhongba, southern Tibet: new constraints on the India-Asia collision. J. Asian Earth Sci. 173, 42–53. https://doi.org/10.1016/j.jseaes.2019.01.012.

Ramstein, G., Fluteau, F., Besse, J., Joussaume, S., 1997. Effect of orogeny, plate motion and land-sea distribution on Eurasian climate change over the past 30 million years. Nature 386, 788–795. https://doi.org/10.1038/386788a0.

Ravikant, V., Wu, F.Y., Ji, W.Q., 2011. U-Pb age and Hf isotopic constraints of detrital zircons from the Himalayan foreland Subathu sub-basin on the Tertiary palaeogeography of the Himalaya. Earth Planet. Sci. Lett. 304, 356–368. https://doi.org/10.1016/j.epsl.2011.02.009.

Raymo, M.E., Ruddiman, W.F., 1992. Tectonic forcing of late Cenozoic climate. Nature 359, 117–122. https://doi.org/10.1038/359117a0.

Richter, F.M., Rowley, D.B., DePaolo, D.J., 1992. Sr isotope evolution of seawater: the role of tectonics. Earth Planet. Sci. Lett. 109, 11–23. https://doi.org/10.1016/0012-821X(92)90070-C.

Rowley, D.B., 1996. Age of initiation of collision between India and Asia: a review of stratigraphic data. Earth Planet. Sci. Lett. 145, 1–13. https://doi.org/10.1016/S0012-821X(96)00201-4.

Royden, L.H., Burchfiel, B.C., van der Hilst, R.D., 2008. The geological evolution of the Tibetan Plateau. Science 321, 1054–1058. https://doi.org/10.1126/science.1155371.

Şengör, A.M.C., Stock, J., 2014. The Ayyubid Orogen: An ophiolite obduction-driven orogen in the Late Cretaceous of the Neo-Tethyan South Margin. Geosci. Can. 41, 225–254. https://doi.org/10.12789/geocanj.2014.41.042.

Spicer, R.A., Su, T., Valdes, P.J., Farnsworth, A., Wu, F.X., Shi, G., Spicer, T.E.V., Zhou, Z., 2021. Why 'the uplift of the Tibetan Plateau' is a myth. Natl. Sci. Rev. 8, nwaa091 https://doi.org/10.1093/nsr/nwaa091.

Su, T., Spicer, R.A., Li, S.H., Xu, H., Huang, J., Sherlock, S., Huang, Y.J., Li, S.F., Wang, L., Jia, L.B., Deng, W.Y.D., Liu, J., Deng, C.L., Zhang, S.T., Valdes, P.J., Zhou, Z.K., 2019. Uplift, climate and Biotic changes at the Eocene-Oligocene transition in Southeast Tibet. Natl. Sci. Rev. 6, 495–504. https://doi.org/10.1093/nsr/nwy062.

Swanson-Hysell, N.L., Fairchild, L.M., Slotznick, S.P., 2019. Primary and secondary red bed magnetization constrained by fluvial intraclasts. J. Geophys. Res. Solid Earth 124, 4276–4289. https://doi.org/10.1029/2018JB017067.

Tahirkheli, R.K., 1979. Geology of Kohistan and adjoining Eurasian and Indo-Pakistan continents, Pakistan. Geol. Bull. Univ. Peshawar 11, 1–30.

Tapponnier, P., Mattauer, M., Proust, F., Cassaigneau, C., 1981. Mesozoic ophiolites, sutures, and large-scale tectonic movements in Afghanistan. Earth Planet. Sci. Lett. 52, 355–371. https://doi.org/10.1016/0012-821X(81)90189-8.

Tapponnier, P., Xu, Z., Roger, F., Meyer, B., Arnaud, N., Wittlinger, G., Yang, J., 2001. Oblique Stepwise rise and growth of the Tibet Plateau. Science 294, 1671–1677. https://doi.org/10.1126/science.105978.

Torsvik, T.H., Cocks, L.R.M., 2017. Earth History and Palaeogeography. Cambridge University Press, Cambridge.

Torsvik, T.H., Van der Voo, R., Preeden, U., Niocaill, C.M., Steinberger, B., Doubrovine, P.V., van Hinsbergen, D.J.J., Domeier, M., Gaina, C., Tohver, E., Meert, J.G., McCausland, P.J.A., Cocks, L.R.M., 2012. Phanerozoic polar wander, palaeogeography and dynamics. Earth-Sci. Rev. 114, 325–368. https://doi.org/10.1016/j.earscirev.2012.06.007.

Van der Voo, R., 1990. The reliability of paleomagnetic data. Tectonophysics 184, 1–9. https://doi.org/10.1016/0040-1951(90)90116-P.

Van der Voo, R., Spakman, W., Bijwaard, H., 1999. Tethyan slabs under India. Earth Planet. Sci. Lett. 171, 7–20. https://doi.org/10.1016/S0012-821X(99)00131-4.

Wan, B., Wu, F., Chen, L., Zhao, L., Liang, X., Xiao, W., Zhu, R., 2019. Cyclical one-way continental rupture-drift in the Tethyan evolution: Subduction-driven plate tectonics. Sci. China Earth Sci. 62, 2005–2016. https://doi.org/10.1007/s11430-019-9393-4.

Wang, C., Zhao, X., Liu, Z., Lippert, P.C., Graham, S.A., Coe, R.S., Yi, H., Zhu, L., Liu, S., Li, Y., 2008. Constraints on the early uplift history of the Tibetan Plateau. Proc. Natl. Acad. Sci. U. S. A. 105, 4987–4992. https://doi.org/10.1073/pnas.0703595105.

Wang, T., Li, G., Aitchison, J.C., Sheng, J., 2020. Eocene ostracods from southern Tibet: implications for the disappearance of Neo-Tethys. Palaeogeogr. Palaeoclimatol. Palaeoecol. 539, 109488 https://doi.org/10.1016/j.palaeo.2019.109488.

Wang, W., Zhang, P., Garzione, C.N., Liu, C., Zhang, Z., Pang, J., Wang, Y., Zheng, D., Zheng, W., Zhang, H., 2022. Pulsed rise and growth of the Tibetan Plateau to its northern margin since ca. 30 Ma. Proc. Natl. Acad. Sci. U. S. A. 119, e2120364119 https://doi.org/10.1073/pnas.2120364119.

Watson, G.S., Enkin, R.J., 1993. The fold test in paleomagnetism as a parameter estimation problem. Geophys. Res. Lett. 20, 2135–2137. https://doi.org/10.1029/93GL01901.

Weller, O.M., Mottram, C.M., St-Onge, M.R., Möller, C., Strachan, R., Rivers, T., Copley, A., 2021. The metamorphic and magmatic record of collisional orogens. Nat. Rev. Earth Environ. 2, 781–799. https://doi.org/10.1038/s43017-021-00218-z.

Westerweel, J., Roperch, P., Licht, A., Dupont-Nivet, G., Win, Z., Poblete, F., Ruffet, G., Swe, H.H., Thi, M.K., Aung, D.W., 2019. Burma Terrane part of the Trans-Tethyan arc during collision with India according to palaeomagnetic data. Nat. Geosci. 12, 863–868. https://doi.org/10.1038/s41561-019-0443-2.

Willems, H., Zhou, Z., Zhang, B., Gräfe, K.U., 1996. Stratigraphy of the upper cretaceous and lower tertiary strata in the Tethyan Himalayas of Tibet (Tingri area, China). Geol. Rundsch. 85, 723–754. https://doi.org/10.1007/BF02440107.

Wu, F.Y., Ji, W.Q., Wang, J.G., Liu, C.Z., Chung, S.L., Clift, P.D., 2014. Zircon U-Pb and Hf isotopic constraints on the onset time of India-Asia collision. Am. J. Sci. 314, 548–579. https://doi.org/10.2475/02.2014.04.

Xiao, W., Ao, S., Yang, L., Han, C., Wan, B., Zhang, J., Zhang, Z., Li, R., Chen, Z., Song, S., 2017. Anatomy of composition and nature of plate convergence: insights for alternative thoughts for terminal India-Eurasia collision. Sci. China Earth Sci. 60, 1015–1039. https://doi.org/10.1007/s11430-016-9043-3.

Xu, Z., Wang, Q., Dong, H., Cao, H., Li, G., Liang, F., Rai, S.M., Kylander-Clark, A., Adhikari, S., Ji, S., 2021. Middle Eocene-Oligocene anatexis and exhumation of the Greater Himalayan Sequence in Central Nepal. Terra Nova 33, 590–601. https://doi.org/10.1111/ter.12551.

Yang, T., Ma, Y., Bian, W., Jin, J., Zhang, S., Wu, H., Li, H., Yang, Z., Ding, J., 2015. Paleomagnetic results from the Early Cretaceous Lakang Formation lavas: Constraints on the paleolatitude of the Tethyan Himalaya and the India–Asia collision. Earth Planet. Sci. Lett. 428, 120–133. https://doi.org/10.1016/j.epsl.2015.07.040.

Yang, Z., Tang, J., Zhao, X., Wang, Y., Santosh, M., Ran, F., Zhang, P., 2022. Direct dating of the Sinongduo thrust system in southern Tibet: immediate response to India-Asia collision. Int. Geol. Rev. https://doi.org/10.1080/00206814.2021.1978110 (In press).

Yin, A., 2006. Cenozoic tectonic evolution of the Himalayan orogen as constrained by along-strike variation of structural geometry, exhumation history, and foreland sedimentation. Earth-Sci. Rev. 76, 1–131. https://doi.org/10.1016/j.earscirev.2005.05.004.

Yin, A., Harrison, T.M., 2000. Geologic evolution of the Himalayan-Tibetan orogen. Annu. Rev. Earth Planet. Sci. 28, 211–280. https://doi.org/10.1146/annurev.earth.28.1.211.

Yuan, J., Yang, Z., Deng, C., Krijgsman, W., Hu, X., Li, S., Shen, Z., Qin, H., An, W., He, H., Ding, L., Guo, Z., Zhu, R., 2021. Rapid drift of the Tethyan Himalaya terrane before two-stage India-Asia collision. Natl. Sci. Rev. 8, nwaa173 https://doi.org/10.1093/nsr/nwaa173.

Zaman, H., Torii, M., 1999. Palaeomagnetic study of Cretaceous red beds from the eastern Hindukush ranges, northern Pakistan: palaeoreconstruction of the Kohistan-Karakoram composite unit before the India-Asia collision. Geophys. J. Int. 136, 719–738. https://doi.org/10.1046/j.1365-246x.1999.00757.x.

Zhang, L., Fan, W., Ding, L., Pullen, A., Ducea, M.N., Li, J., Wang, C., Xu, X., Sein, K., 2022. Forced subduction initiation within the Neotethys: an example from the mid-Cretaceous Wuntho-Popa arc in Myanmar. Geol. Soc. Am. Bull. 134, 849–870. https://doi.org/10.1130/B35818.1.

Zhang, P., Molnar, P., Downs, W.R., 2001. Increased sedimentation rates and grain sizes 2-4 Myr ago due to the influence of climate change on erosion rates. Nature 410, 891–897. https://doi.org/10.1038/35073504.

Zhang, P.Z., Shen, Z., Wang, M., Gan, W., Bürgmann, R., Molnar, P., Wang, Q., Niu, Z., Sun, J., Wu, J., Sun, H., You, X., 2004. Continuous deformation of the Tibetan Plateau from Global Positioning System data. Geology 32, 809–812. https://doi.org/10.1130/G20554.1.

Zhang, W., Fang, X., Zhang, T., Song, C., Yan, M., 2020. Eocene rotation of the northeastern central Tibetan Plateau indicating stepwise compressions and eastward extrusions. Geophys. Res. Lett. 47, e2020GL088989 https://doi.org/10.1029/2020GL088989.

Zhao, Y., Tzedakis, P.C., Li, Q., Qin, F., Cui, Q., Liang, C., Birks, H.J.B., Liu, Y., Zhang, Z., Ge, J., Zhao, H., Felde, V.A., Deng, C., Cai, M., Li, H., Ren, W., Wei, H., Yang, H., Zhang, J., Yu, Z., Guo, Z., 2020. Evolution of vegetation and climate variability on the Tibetan Plateau over the past 1.74 million years. Sci. Adv. 6, eaay6193 https://doi.org/10.1126/sciadv.aay6193.

Zheng, H.B., Yang, Q., Cao, S., Clift, P.D., He, M.Y., Kano, A., Sakuma, A., Xu, H., Tada, R., Jourdan, F., 2022. From desert to monsoon: irreversible climatic transition at ~36 Ma in southeastern Tibetan Plateau. Prog. Earth Planet. Sci. 9, 12. https://doi.org/10.1186/s40645-022-00470-x.

Zhou, S., Mo, X., Dong, G., Zhao, Z., Qiu, R., Guo, T., Wang, L., 2004. 40Ar-39Ar geochronology of Cenozoic Linzizong volcanic rocks from Linzhou Basin, Tibet, China, and their geological implications. Chin. Sci. Bull. 49, 1970–1979. https://doi.org/10.1007/BF03184291.

Zhu, D., Wang, Q., Zhao, Z., 2017. Constraining quantitatively the timing and process of continent-continent collision using magmatic record: Method and examples. Sci. China Earth Sci. 60, 1040–1056. https://doi.org/10.1007/s11430-016-9041-x.

Zhu, D.C., Wang, Q., Zhao, Z.D., Chung, S.L., Cawood, P.A., Niu, Y., Liu, S.A., Wu, F.Y., Mo, X.X., 2015. Magmatic record of India-Asia collision. Sci. Rep. 5, 14289. https://doi.org/10.1038/srep14289.

Zhu, R., Zhao, P., Zhao, L., 2022. Tectonic evolution and geodynamics of the Neo-Tethys Ocean. Sci. China Earth Sci. 65, 1–24. https://doi.org/10.1007/s11430-021-9845-7.

Zhuang, G., Najman, Y., Guillot, S., Roddaz, M., Antoine, P.O., Métais, G., Carter, A., Marivaux, L., Solangi, S.H., 2015. Constraints on the collision and the pre-collision tectonic configuration between India and Asia from detrital geochronology, thermochronology, and geochemistry studies in the lower Indus basin, Pakistan. Earth Planet. Sci. Lett. 432, 363–373. https://doi.org/10.1016/j.epsl.2015.10.026.